THE INFLUENCE OF MECHANICAL VIBRATION ON FREE CONVECTIVE HEAT TRANSFER FROM HORIZONTAL CYLINDERS

EDWARD M. PEEBLES

THE INFLUENCE OF MECHANICAL VIBRATION ON FREE CONVECTIVE HEAT TRANSFER FROM HORIZONTAL CYLINDERS

by

LIEUTENANT EDWARD M. PEEBLES, U.S. NAVY

B.S., UNITED STATES NAVAL ACADEMY
(1955)

SUBMITTED IN PARTIAL FULFILLMENT OF THE REQUIREMENTS

FOR THE DEGREES OF

NAVAL ENGINEER AND MASTER OF SCIENCE

at the

MASSACHUSETTS INSTITUTE OF TECHNOLOGY

June 1961

THE INFLUENCE OF MECHANICAL VIBRATION ON FREE CONVECTIVE HEAT TRANSFER FROM HORIZONTAL CYLINDERS

by

Lieutenant Edward M. Peebles, USN

Submitted to the Department of Naval Architecture and Marine Engineering on May 20, 1960 in partial fulfillment of the requirements for the Master of Science Degree in Naval Architecture and Marine Engineering and the Professional Degree, Naval Engineer.

ABSTRACT

This thesis is a report of an experimental investigation of the influence of horizontal mechanically induced simple harmonic vibrations upon the rate of heat transfer by free convection from a horizontal heated cylinder to air. The diameter of the cylinder was 7/8", and the ranges of the principal experimental variables were as follows:

temperature potential, Δt:	$150^{\circ}F \pm 1^{\circ}F$
frequency of vibration, f:	104 cps
amplitude of vibration, a:	0.025 to 0.128"
intensity of vibration, af:	0.21 to 1.11 ft/sec

The data show that the influence of vibrations upon the heat-transfer coefficient is negligible for intensities of vibration, af, less than 0.3 ft/sec; above this so-called "critical intensity," the effect of vibrations is to increase the heat-transfer coefficient significantly. The quantitative heat transfer results of this investigation show close agreement with the results reported for horizontal cylinders in the presence of high intensity horizontal sound fields. An elementary flow-visualization examination utilizing smoke was performed which indicated that the free convective flow near the lower test cylinder stagnation point remained laminar in the presence of vibrations. The quantitative heat transfer results, supported by the flow study, lead to the conclusion that the physical mechanism of heat transfer for mechanically induced horizontal vibration of a cylinder is the same as for acoustically induced horizontal vibrations in the fluid medium surrounding the cylinder. The close quantitative agreement of the results for the two methods of vibration also indicates that the influence of the amplitude of vibration to cylinder diameter ratio, a/D_0, which differed by a factor of 12.3, is not significant for the range of a/D_0 ratios considered.

Thesis Supervisor: George A. Brown

Title: Assistant Professor of Mechanical Engineering

ACKNOWLEDGMENTS

The thesis supervisor for the greater portion of this project was the late Professor Joseph Kaye. The author wishes to express his appreciation to Professor George A. Brown for accepting the supervisorship for the conclusion of the project.

The author is greatly indebted to Dr. Richard M. Fand, Executive Officer, Research Laboratory of Heat Transfer in Electronics, M.I.T. for the design of the special heat transfer test cylinder, and for his generous guidance and encouragement throughout all phases of the project. Credit is due Mr. Charles Teleki for the design of the test cylinder support yoke used in the experiments.

TABLE OF CONTENTS

LIST OF FIGURES

LIST OF TABLES

LIST OF SYMBOLS

Latin Letters

a	single amplitude of vibration, in
af	product of amplitude times frequency, called the vibration intensity, ft/sec
A	heat transfer surface area, ft^2 or beam cross-sectional area, in^2
b	beam width, in
D_o	test cylinder diameter, in
e	surface thermal emissivity, dimensionless
E	Young's modulus of elasticity, lb/in^2
f	frequency of vibration, cps
g_o	gravitational constant, in/sec^2
h	beam height, in
h_o	heat-transfer coefficient in absence of vibrations, $Btu/hr\text{-}ft^2\text{-}^oF$
h_v	heat-transfer coefficient in presence of vibrations, $Btu/hr\text{-}ft^2\text{-}^oF$
I	cross-sectional moment of inertia, in^4
ℓ	beam half-length, in
m_b	beam mass, $lb\text{-}sec^2/in$
m_c	beam center-span mass, $lb\text{-}sec^2/in$
M	bending moment, in-lb
Q_{co}	heat transferred by convection in the absence of vibration, watts
Q_{cv}	heat transferred by convection in the presence of vibration, watts

Q_d	heat loss by conduction to test cylinder supports, watts
Q_m	indication of wattmeter in test section heater circuit, watts
Q_r	heat transferred by radiation, watts
Q_{uo}	unaccountable heat loss in absence of vibration, watts
Q_{uv}	unaccountable heat loss in presence of vibration, watts
Q_w	heat delivered to test section, watts
t	time, sec
t_a	ambient temperature, ^oF
t_b	mean ambient temperature, ^oF
t_s	surface temperature, ^oF
Δt	temperature potential, $\Delta t = t_s - t_a$, ^oF
Δt_{hm}	heat meter temperature differential, ^oF
U_1	defined by Equation (32), Appendix A
U_2	defined by Equation (33), Appendix A
U_3	defined by Equation (34), Appendix A
W_b	beam weight, lbs
W_c	beam center-span load, lbs
x	distance along beam, in
x_n	distance of vibration node from beam end, in
y	beam displacement, in

Greek Letters

α	defined by Equation (18), Appendix A
γ	beam weight density, lb/in^3
π	mathematical constant, $\pi = 3.1416$
σ	Stefan-Boltzman constant, $\sigma = 0.1713 \times 10^{-8}$ Btu/hr-ft^2-$^\circ$F
σ_{max}	maximum bending stress in beam, lb/in^2
ω	circular frequency, rad/sec

CHAPTER I

INTRODUCTION

The study of heat transfer in the presence of vibrations is a relatively new area of investigation that has received increasing attention in recent years. Several experimental investigations have indicated a marked increase in convective heat-transfer rates in the presence of strong vibrations. Since heat transfer is a limiting factor in many areas of engineering design, it is important to account for the effects of vibration on heat transfer where vibration is present. In certain cases, advantage may be taken of increased heat-transfer rates to render certain heat-transfer dependent processes more efficient. As an example, Raben and Dietert (1) have conducted an investigation designed to use vibrations to increase heat-transfer rates in a saline water conversion process.

The influence of vibrations upon the free convective heat-transfer rate from a heated surface can be investigated experimentally by two different methods. In one method the heated surface is held stationary within a fluid medium. An oscillatory motion is impressed upon this fluid medium -- that is, this method requires the establishment of a sound field in the vicinity of the heated surface and will, therefore, be referred to subsequently as the "sound method." An alternate experimental approach is to impress a vibratory motion on the heated surface itself, leaving the fluid medium surrounding the surface otherwise undisturbed. This second method generally employs a resonant mechanical system to achieve sustained vibrations of the heat-transfer surface and will, therefore, be referred to as the "mechanical vibrations method." The objective achieved by the two

methods is identical. That is, the relative velocity vector between the fluid medium and the heated surface undergoes a periodic change of magnitude and sign. Indeed, an analytical study[2] has shown that, for sufficiently long wave-lengths, identical fluid flows should exist near a surface if the direction, amplitude, and frequency of vibration are the same, regardless of which of the two methods is used to create the vibration.

An early attempt to correlate the effects of vibration on heat transfer is that of Martinelli and Boelter[3]. In this investigation, a 3/4" diameter horizontal electrically heated tube, immersed in water, was subjected to vertical sinusoidal vibration. Amplitudes up to 0.10" and frequencies up to 40 cps were employed. The range of temperature potential, Δt, extended from 8 to 45°F. No influence on the heat-transfer coefficient was observed in the lower range of vibration Reynolds number; this result was attributed to the dominance of free convection in this range. At higher vibration Reynolds numbers, however, a gain of as much as 400 per cent relative to the non-vibration case was observed. Unfortunately, Boelter, in a communication to Lemlich[4], has reported that these results could not be verified in a later series of experiments.

The effect of vibrations on convective heat-transfer rates from horizontal wires to air has been studied by Lemlich[4]. Three heated wires of varying diameter (0.0253", 0.0396" and 0.0810") were set in vibration at frequencies between 39 and 122 cps with a maximum amplitude of 0.115". Increases in the heat-transfer rates were reported for increases in frequency or amplitude. Improvements in heat-transfer coefficients by as much as a factor of four were reported. In addition, Lemlich reported similar results

for both vertical and horizontal vibrations and concluded that the variation in heat transfer was independent of the direction of vibration.

Tsui[5] has conducted an experimental investigation of the effect of transverse vibrations on the heat-transfer rate from a heated vertical plane surface. Increases in heat-transfer coefficients up to 25 per cent were noted. Tsui attempted to treat the system analytically, but concluded that the general equations correlating vibration and heat transfer are insolvable with present techniques. Shine[6] performed experiments similar to those of Tsui. A heated vertical plate was subjected to transverse vibrations of 11 to 315 cps at amplitudes up to 0.061". Plate temperature range was from 131 to 279°F. Significantly, these tests demonstrated that as the amplitude-frequency product, af, (arbitrarily defined as the vibration intensity) was increased, the heat transfer was not affected until a specific value of af was reached. Above this "critical" vibration intensity, af = 0.083 ft/sec, the rate of heat transfer increased markedly.

Freedman[7] has investigated the case of a vertical heated cylinder vibrating in an axial direction. No change in heat-transfer rate was noted over the range of vibration intensities achieved (maximum vibration intensity, af = 0.2 ft/sec).

Fand, Kaye and Teleki[8, 9] have recently conducted experimental investigations of the influence of vertical mechanical vibrations (Fig. 1-b) upon the heat-transfer rate by free convection from a heated horizontal cylinder to air. The diameter of the cylinder was 7/8", and the ranges of the variables were as follows: temperature potential, Δt, 25 to 185°F; amplitude of vibration, a, 0 to 0.16"; frequency of vibration,

f, 54 to 225 cps; and intensity of vibration, af, 0 to 1.22 ft/sec. These authors report that the sole controlling vibrational variable is the vibration intensity, af. Further, the critical value of af was about 0.3 ft/sec. A flow-visualization study using smoke indicated that the fluid-dynamical mechanism which causes the increase in heat transfer rate is vibrationally induced turbulence.

An extensive investigation involving the sound method, that is, the effect of sound fields upon the heat transfer by free convection from a stationary horizontal cylinder to air, has been reported by Fand and Kaye[10]. In their experimental arrangement the sound vibration vector was normal to both the cylinder axis and the gravity field (Fig. 1-a). The frequency range covered was from 1100 to 6120 cps; the vibration intensity range was from 0 to 1.3 ft/sec; and the temperature potential was varied from 0 to 250°F. A critical vibration intensity of approximately 0.3 ft/sec was observed; below this intensity the heat-transfer coefficient was unaffected. The data also showed that for sound waves whose half wavelength was six or more times the test cylinder diameter, the heat-transfer coefficient is a function of only two variables; namely, the temperature potential, Δt, and the vibration intensity, af. In the tests above the critical intensity the rate of heat transfer increased rapidly until an af of about 0.6 ft/sec was reached; above this intensity level the rate of change of heat transfer was less rapid and could be expressed by the following algebraic expression:

$$h_v = 0.722 \left[\Delta t \, (af)^2 \right]^{1/3} \qquad (1)$$

where h_v is the coefficient of heat transfer in the presence of vibrations, Btu/hr-ft^2-$^\circ$F; af is the vibration intensity, ft/sec; and Δt is the temperature potential, $^\circ$F.

Fand and Kaye[11] examined the physical mechanism which caused the heat-transfer rate to increase in the presence of sound by means of a smoke flow-visualization technique. This study showed that at the critical sound intensity the typical free-convective boundary-layer flow pattern around the heated cylinder is disrupted, and a fundamentally different type of boundary-layer flow, called thermoacoustic streaming,develops. This thermoacoustic streaming appears as a special type of vortex motion. In the presence of both horizontal vibration and a temperature gradient, a pair of vortices alternately form in the two quadrants above the heated cylinder surface. The inception of this oscillating vortex pair formation occurs at the critical vibration intensity, and the further development of these vortices corresponds to that range of af wherein the heat-transfer coefficient increases most rapidly. A further increase in the vibration intensity serves to more fully develop these vortices, but does not alter their form.

The investigations summarized above have, for the most part, been of an experimental nature. All attempts to obtain a general analytical solution to the problem have been unsuccessful thus far. In view of this, it appears necessary to add to the knowledge of the physical relationships between vibrations and heat transfer by empirical means. The primary consideration involved in the experimental program undertaken in this

work is to establish the heat-transfer behavior of horizontal cylinders under horizontal mechanically induced sinusoidal vibration, where the vibration vector and the force of gravity are in the same relationship to a heated test cylinder as in the sound investigations of Fand and Kaye. No direct comparison of the sound method and the mechanical vibrations method with both the test cylinder axis and the vibration vector normal to the direction of the gravity field (Fig. 1-a) has been reported. As noted above, investigations made of the influence of vertical vibrations on the heat-transfer rate of a horizontal cylinder to air (Fig. 1-b) have indicated that the basic mechanism of convective air flow around the cylinder is vibrationally induced turbulence, not thermoacoustic streaming as observed in the sound method. Therefore, it was desired to determine if the character of heat transfer and the associated thermoacoustic streaming phenomenon exhibited in the sound method can be related to the mechanical vibrations method. Accordingly, this study is an experimental investigation of the influence of horizontal mechanically induced simple harmonic vibrations upon the heat-transfer rate by free convection from a heated horizontal cylinder to air.

CHAPTER II

GENERAL DISCUSSION OF EXPERIMENTAL DESIGN

The primary objective of this investigation was to determine experimentally the influence of transverse horizontal mechanically induced simple harmonic vibrations upon the heat-transfer rate by free convection from a heated horizontal cylinder to air. This configuration (Fig. 1-a) was chosen in order to provide direct comparison with available data for stationary horizontal cylinders in the presence of transverse horizontal sound fields. In particular, the experimental program was designed to establish whether or not a quantitative comparison of the heat-transfer variation for the two cases at identical temperature potentials, Δt, and intensities of vibration, af, does in fact exist. To this end, then, the following experimental goals were established:

a. To construct a mechanical vibratory system which, at resonance, could drive the test cylinder at vibrational intensities, af, up to 1.50 ft/sec
b. To provide a suitable means to measure vibration amplitude and frequency accurately
c. To construct a heat transfer test cylinder which could operate under the imposed vibration at surface temperatures up to 350^{o}F
d. To provide a power supply to heat the test cylinder and a temperature measuring system for accurate temperature measurement of the test cylinder surface.

Based on the experience of others[8, 9], it was determined that the test cylinder should be rigidly coupled to a resonant mechanical system. At resonance the force magnification factor could be utilized for obtaining maximum vibrational amplitude. Also, although the test program contemplated here involved only horizontal vibrations, it was considered economical to design the vibration test equipment with a view toward future work employing other vibration directions. Hence, it was decided to incorporate into the vibration system means by which the vibration direction could be varied from 0 to 90° with respect to the direction of the force of gravity.

The basic element of the mechanical system chosen to provide vibration was a simple free-free beam as shown in Fig. 2. The free-free beam offers the advantage of confining the major forces, which are the inertia forces, to the beam itself and not to the supporting structure. Supporting the free-free beam at the nodal points minimizes any hysteresis losses in the supports since there is no force transmission to the supports. Therefore, less energy absorption occurs at the nodal supports than would occur, for example, at the supports of a clamp-clamp or hinge-hinge beam.

The test cylinder was rigidly connected to the test cylinder by means of a yoke. The beam itself was supported at the nodes by a "gimbal" arrangement attached to a rigid "alignment platform" as shown in Figs. 2 and 3. The distance between the gimbal supports could be varied to the computed nodal positions of the beam when the beam was placed in resonant vibration. The alignment platform was attached to a MB Electronics Model CIF Vibration Exciter which provided the external driving force. The motion of the test cylinder resulting from an electric excitation of the

coupled dynamic system was a uniform, one-dimensional sinusoidal transverse vibration. The frequency of vibration employed was 104 cps; however, beams designed for other resonant frequencies could be used, as provision was made for fitting beams of variable dimensions into the vibration test stand. Vibration amplitude was measured by a cathetometer.

The test cylinder, which was heated by an internal electrical heater, had a diameter of 7/8". Test cylinders previously used in other experiments[8, 9] involving heat transfer under conditions of vibration employed guard heaters on either side of the central test section heater in order to eliminate the problem of axial heat conduction away from the test section. The complexity resulting from this type of construction -- that is, the use of three interconnecting parts, each with its own heating element and thermocouple arrangement -- has resulted in premature failure by fatigue. In order to avoid fatigue failure, the test cylinder for this project was designed with one heater; a metering device was installed at each end of the cylinder to measure the axial conduction heat losses to the test cylinder supports.

A total of eight thermocouples were installed in the test cylinder for surface temperature measurement. The location of these thermocouples is as shown in Fig. 5. Each copper-constantan thermocouple was encapsulated in the end of a copper-plated stainless steel tube. The tube was then closely fitted into its individual hole drilled axially into the cylinder wall. Thus the thermocouples were firmly fixed in position, and a good thermal contact between the junctions and the cylinder was established.

There was an obvious danger of test cylinder lead-wire breakage under vibrationally induced loads as high as 200 g's during the course of the tests. Several special techniques were used to avoid wire breakage and are described in detail in Chapter V, Section 1-c.

The vibration test stand itself was located in a special test room 8 x 13 x 15' high. A 4 x 6' glass window was placed in the wall between the test stand and the adjacent control room. Thus, optical amplitude measurements and all other test operations could be conducted without disturbing the air in the vicinity of the test cylinder.

CHAPTER III

APPARATUS

The apparatus can be conveniently divided into two basic categories with subdivisions as follows:

1. Vibration Apparatus
    - 1-a. General
    - 1-b. Resonant beam
    - 1-c. Test stand
    - 1-d. Vibration exciter and exciter power supply
    - 1-e. Amplitude and frequency measuring apparatus
2. Heat Transfer Apparatus
    - 2-a. General
    - 2-b. Test cylinder
    - 2-c. Power supply
    - 2-d. Temperature measuring apparatus

1. Vibration Apparatus

1-a. General

In order to produce the intensities of vibration required for this investigation, it was necessary to employ a mechanical resonant system. This was evident from the characteristics of the available vibration exciter; the maximum acceleration obtainable from this exciter, using direct force take-off, was about 75 g's. As stated in Chapter II, acceleration loads up to approximately 200 g's were required to obtain the

desired value of af = 1.5. To obtain these high accelerations, it was necessary to interpose a mechanical resonant system between the vibration exciter and the test cylinder. This is the general technique described in the literature used to produce high values of vibration intensity.

An additional requirement of the vibration system was that the vibration motion produced had to be sinusoidal and one-dimensional in character. This requirement restricted the selection of the resonant system to one which would vibrate essentially in its first natural mode with negligible effect from any higher harmonics. A prismatical beam was the system chosen which satisfied both the resonance and sinusoidal, one-dimensional motion requirements.

Other mechanical resonant systems could have been devised to produce the motion required -- such as a system using heavy coiled springs, for example. However, the simple geometry of the rectangular beam lends itself more conveniently to accurate analysis, design and construction.

Resonant beam vibration with clamp-clamp, hinge-hinge and free-free boundary conditions were investigated. The free-free vibration of a beam in the first mode was selected as the preferable method for obtaining the required vibration intensity because this system exhibits the least damping. In free-free beam vibration the major forces, which are the inertia forces, are balanced within the beam itself and not transmitted to the structure supporting the beam. Thus, the joint type of damping loss is eliminated. An additional advantage results from this absence of major force transmission at the supports: the supporting structure is largely free of induced vibrations and can be designed accordingly.

One disadvantage in employing a free-free resonant beam compared to a clamp-clamp resonant beam is the necessity to provide a different beam for each vibration frequency desired. However, since it has been demonstrated by other investigators[8, 9] that the sole vibrational variable affecting heat-transfer rates is the intensity of vibration -- the amplitude-frequency product, af. Hence, it is possible to investigate the influence of vibration intensity on heat transfer by varying the amplitude of vibration at constant frequency.

1-b. Resonant beam

The complete analysis of the free-free beam with center-span test cylinder load is given in detail in Appendix A. The results and interpretation of this analysis are presented here.

In the analysis it was assumed that the beam at its resonant frequency, has a motion essentially of the first mode only, the effects of the higher harmonics being negligible. This assumption is considered valid for a uniform, carefully machined, prismatical beam. Further, tests showed that the vibratory motion of the beam was, in fact, sinusoidal and one-dimensional in character.

The resonant frequency equation of the system, as derived in Appendix A, in terms of beam mass, m_b, and the mass at beam center-span, m_c, is:

$$\frac{m_b}{m_c} = - \frac{\alpha l \, (\operatorname{sech} \alpha l + \cos \alpha l)}{(\sin \alpha l + \cos \alpha l \tan h \alpha l)} \qquad (2)$$

where l is one-half the beam length and α is defined as:

$$\alpha^4 = \frac{12 \gamma}{E g_c} \left(\frac{\omega}{h}\right)^2$$

E = modulus of elasticity, lb/in^2

g_o = gravitational constant, in/sec^2

γ = beam weight density, lb/in^3

ω = circular frequency, rad/sec

h = beam height in motion direction, in

Equation (2) is plotted in Fig. 6.

In terms of the beam physical parameters, the resonant frequency can be expressed as:

$$f = \frac{1}{2\pi} \left(\frac{g_o}{12}\right)^{1/2} \left(\frac{E}{\gamma}\right)^{1/2} \alpha^2 h \qquad (3)$$

Therefore, for a beam of given dimensions, the vibration intensity is:

$$af = \text{Constant} \times a \times \left(\frac{E}{\gamma}\right)^{1/2} \qquad (4)$$

Consideration of maximum bending stress leads to the following relationship between maximum bending stress in the beam, σ_{max}, and amplitude of vibration, a, as derived in Appendix A and plotted in Fig. 9:

$$\frac{\sigma_{max}}{a} = \frac{E}{2} \frac{h}{l^2} \text{ (a function of } \alpha l \text{)} \qquad (5)$$

Equations (2), (4) and (5) form the essential basis for resonant free-free beam selection. Fig. 9 clearly shows that a high value of αl is desired in order to minimize bending stress in the beam, and Fig. 6 indicates that large values of αl correspond to large values of the beam mass to center load mass ratio, m_b/m_c. The weight of the center load was known to be approximately 5.5 lbs. This weight included the weights of all the

moving parts attached to the center of the beam: the test cylinder yoke, the moving element of the vibration exciter, and the parts used to couple the vibrator moving element and test cylinder yoke to the beam. Therefore, it is clear from Fig. 6 that for a reasonable beam size, the value of αl would have to be within the range of about 2.20 to 2.28. These values of αl represent beam weights from 19 lbs to 52 lbs as obtained from Fig. 6, using a value for center-span load of 5.5 lbs. In the actual beam selection a compromise value of $\alpha l = 2.25$ and a corresponding beam weight of 31.6 pounds were used for purposes of analysis. A lower value of αl would impose a greater bending stress, and a higher value of αl would require a beam larger than could be conveniently used.

Equation (4) indicates that a high value of E/γ is desired.

Additional considerations involved in the beam design include the vibration frequency and fatigue strength. The frequency at which resonance was desired was in the neighborhood of 100 cps. This frequency was selected as being high enough to be well within the frequency ranges used by other investigators to demonstrate marked effects of vibration on heat-transfer rates, and low enough to avoid more severe inertia loads at yet higher frequencies. The loading is proportional to the square of the frequency, and even at frequencies of 100 cps, inertia loads of about 200 g's were anticipated. The vibration test stand was designed so that beams of varying dimensions could be installed; hence, frequency could be varied by changing beam size.

Fatigue strength was a primary factor involved in beam material selection. The beam was required to sustain complete stress reversals for long periods of time. Beam failure might have resulted in test

cylinder destruction or, at least, would have caused considerable delay in the test program.

Of the several beam materials considered, aluminum and steel were given consideration based on strength and fatigue characteristics, availability, machinability, and the requirement of Equation (4), namely, a high E/γ ratio. From the stress standpoint, the best available aluminum alloy was 2024-T4, a special heat-treated alloy which has a yield stress of 50,000 lb/in^2, and the best available steel alloy was a special treatment steel, "HY-100," which has a yield stress in excess of 100,000 lb/in^2.

The endurance limit for Al 2024-T4 is quoted as 20,000 lb/in^2. This is an arbitrarily defined endurance limit, for it is well known that the fatigue characteristics of non-ferrous metals do not exhibit a limiting value of fatigue strength below which the material strength is independent of the number of stress cycles. No fatigue data for HY-100 steel is currently available. It is known that the endurance limit for most alloy steels is approximately one-half the yield strength; therefore, "HY-100" steel was considered to be adequate from the fatigue standpoint up to stress levels of approximately 50,000 lb/in^2.

Each of these two metals could be machined readily; and aluminum and steel have about the same E/γ ratios -- 1.0×10^8 and 1.1×10^8 inches, respectively -- giving each material about the same footing relative to the requirement of Equation (4).

The width, b, of the beam was established as 1.50" initially in order that existing test cylinder support equipment could be used. In a study made of Al 2024-T4 and HY-100 beams, the first comparison was made on the

basis of equivalent beam size, and the second comparison was made for identical values of αl . The results of the equal beam size calculations made in accordance with the method given in Appendix B were:

Beam Size -- 1.50" x 1.44" x 52,00"

	αl	f(cps)	af (ft/sec)	σ_{max} (lb/in^2)
Steel	2.25	100	1.50	52,000
Aluminum	2.15	100	1.50	25,500

The results of the comparison on the basis of identical values of were:

	Size	αl	f(cps)	af (ft/sec)	σ_{max} (lb/in^2)
Steel	1.50"x1.44"x52.00"	2.25	100	1.50	52,000
Aluminum	1.50"x2.90"x73.00"	2.25	100	1.50	18,000

These figures indicate, for αl = 2.25, that either material would be satisfactory. Considering the superior fatigue characteristics of steel as compared to aluminum, however, HY-100 was selected as the beam material for the final design.

The HY-100 obtained for the project had the following alloy content (MIL-S-20154A):

Carbon	Nickel	Chromium	Molybdenum
0.20-0.21	3.50	1.50	0.40

Two standard tensile specimen tests gave the following results:

	No. 1	No. 2
Yield strength (lb/in^2)	106,000	102,200
Ultimate strength (lb/in^2)	124,300	111,900

The dimensions and characteristics of the beam used in the test stand were as follows:

width, b	height, h	length, 2l	f (calc.)	f (actual)	αl
1.474"	1.408"	50.00"	105.3 cps	104cps	2.243

Small variations from the planned dimensions were necessary because of the machining required to produce a straight beam with a 63 micro-inch finish from the available stock. In addition, the length of the beam was adjusted to raise the calculated resonant frequency somewhat above 100 cps to allow for the added mass of the gimbals mounted at the beam nodes and because the weight placed at beam center span was not accurately known until all parts were constructed. The measured resonant frequency was about 1 per cent less than the calculated value.

1-c. Test stand

The vibration test stand and its components are shown in Figs. 2, 3 and 4. The purpose of the test stand was to provide a means of support for the resonant beam and a method for accurate alignment of the resonant beam with respect to the vibration exciter.

Resonant beam support at the nodes of vibration was accomplished by two gimbal assemblies. At each node an aluminum gimbal frame was fitted to the resonant beam by means of a stainless steel slipper. The beam

slipper was incorporated into the gimbal design so that beams of different sizes could be fitted into the gimbal frame -- that is, each beam with its own pair of slippers could rest in the existing gimbal frames. A beam clamp plate served to hold the beam firmly within the gimbal frame by means of two 1/4" set screws and lock-nuts. To allow for gimbal frame oscillatory rotation caused by beam deflection during vibration, hardened steel journals were fitted into both sides of the gimbal frame at its axis of rotation. The journals were first put through the holes in the gimbal supports and then seated in the gimbal frame holes with 5/16" shoulder bolts. Operation of the apparatus later indicated that the journals came loose in the gimbal frame holes, causing local heating and eventual seizure of the frame within the gimbal supports. To correct this situation, each journal was keyed to the gimbal frame, effectively preventing any relative motion between the journal and gimbal frame. In addition, a journal oil supply system was installed; oil cups were mounted on top of each gimbal support post with oil wicks leading down to the journal through holes in these support posts. To distribute the oil around the journal, a circumferential 1/16" x 1/16" groove was milled in the center of the 9/16" diameter hole of each gimbal support post. A 10 per cent colloidal dispersion of molybdenum-disulfide in oil was used as the lubricant.

Each gimbal assembly was secured to an alignment platform by four 3/8" bolts. Since the nodal position was located by calculation (see Appendix A), small errors in gimbal frame mounting position did exist. Thus, some vertical force was applied to the gimbal supports. A rigid connection of the gimbal assembly to the alignment platform would have

introduced a significant amount of damping. Therefore, provision for small relative motion between the gimbal assembly and the alignment platform was made by placing a 1/32" sheet of neoprene rubber between them.

The alignment platform was designed to insure accurate alignment of the resonant beam with respect to the vibration exciter driver axis. Accurate positioning of the resonant beam was necessary so that no lateral force component could be applied to the exciter driver coil through the exciter extension. Clearance between the exciter driver and field coils was such that any misalignment of the exciter extension could cause the driver coil to come in damaging contact with the field coil. The alignment platform, machined from a standard 8" structural channel section, was slotted along the top center-line to receive the pad projections of the gimbal supports. This arrangement prevented any lateral motion of the resonant beam. To facilitate moving the gimbal assemblies to the resonant beam node positions four slots, 16" in length, were machined in the alignment platform.

Small stainless steel bench marks were located on the alignment platform on either side of the central 1 3/8" diameter hole for the aluminum exciter extension. These bench marks served as a convenient aid in locating the gimbal assemblies at equal distances from the beam center.

A special brass alignment plug was made to fit into the 1 3/8" diameter hole through which the exciter extension was centered. The alignment plug had its center drilled out to the exact diameter of the exciter extension. Thus, the installation position of the alignment platform on the vibration exciter was accurately determined when the

alignment plug, with the exciter extension through its center, would just slide into the 1 3/8" diameter hole in the center of the alignment platform.

The alignment platform was attached to the vibration exciter by quadrants and brackets in an arrangement which permitted rotation of the entire exciter-alignment platform portion of the test stand relative to the exciter base. In this manner the direction of vibration could be varied 0 to 90° relative to the direction of gravity. The brackets were bolted to the top face of the exciter casting, and the quadrants were fitted to the same trunnions which normally connect the exciter to its base.

The exciter base was in turn bolted to a 2' section of 14" x 14 1/2" wide-flange beam which served as the base support for the entire vibration test stand, as shown in the photograph, Fig. 10. Adjustable legs were installed at each corner of the wide-flange base to provide a convenient means of leveling the test stand. These legs supported the base through 4" square pads of heavy rubber which prevented vibration transmission to the test room floor.

The yoke which held the test cylinder at mid-span of the resonant beam was a U-shaped, finned structure which combined high rigidity with minimum weight. The base plate of the test cylinder yoke was held to the resonant beam by means of a steel clamping plate. The resonant beam was firmly clamped between these two plates held together by four 1/4" steel bolts. A calculation of stresses showed that the maximum stresses in these bolts during vibration were at all times well below the allowable limit. To prevent any corrosive or cutting action between the plates and the

resonant beam, thin pieces of Teflon sheet were placed between the plates and the beam.

The lead wires of the test cylinder were fastened to the test cylinder in the manner described in section 2-b of this chapter. These wires were brought down along the test cylinder yoke and taped to the resonant beam as seen in Fig. 11. The lead wires were held firmly along the yoke by taping them to a stiff U-shaped wire which was anchored to the yoke at both ends and at the center of the resonant beam as can be seen in the close-up photograph, Fig. 11. The wires were then taped along the side of the beam and led off the beam near the nodes to cable clamps fitted with rubber grommets on the gimbal support posts. This arrangement prevented any large relative motion between adjacent parts of the wires, and lead wire breakage was avoided completely.

1-d. Vibration exciter and exciter power supply

The external driving force for vibration at resonance was supplied by a MB Electronics Model C1F electrodynamic vibration exciter. The sinusoidal force output of this exciter was 50 lbs maximum within a frequency range of 6 to 350 cps. Driver coil motion was limited to a double amplitude of 1/2"; an over-travel limit switch was provided to open the driver coil circuit in case this limit was exceeded. The force generated was directly proportional to the value of alternating current in the driver coil for constant direct current input to the field coil. The force rating of the exciter with 1.75 amperes input to the field coil was 10 lbs vector force for each 1.0 ampere r.m.s. of alternating current applied to the driver coil. The maximum driver coil current was 5.0 amperes.

The power supply for the vibration exciter was the associated MB Electronics Model T112031 Power Supply. This power console contained an audio-oscillator with amplifier which supplied a sinusoidal wave form current to the driver coil and included built-in impedance matching controls. The field coil supply in the console was a rectifier which provided direct current up to the rated 1.75 amperes for the exciter field coil.

1-e. Amplitude and frequency measuring apparatus

The vibration amplitude of the test cylinder was measured optically by sighting through a cathetometer on a specially made target. The target consisted of a short piece of 0.001" diameter wire mounted on a black background. When the target was illuminated by an intense spotlight, the image visible through the cathetometer microscope was a thin bright line corresponding to the sharply illuminated crest of the wire. When the cylinder was put into vibration, this image became a bright distinct band with a width equal to the double amplitude of vibration. The accuracy of amplitude measurement was better than 0.002".

Frequency measurement was obtained by feeding a signal from the audio-oscillator in the exciter driver coil circuit into a Hewlett Packard Model 521A Electronic Counter. The counter frequency reading was always in good agreement with the calibrated dial of the audio-oscillator; the accuracy of the frequency measurement was within ± 1 per cent.

2. Heat Transfer Apparatus

2-a. General

The heat transfer apparatus consisted of a test cylinder, a power supply to heat the test cylinder and a system of thermocouples installed in the test cylinder for surface temperature measurement. Special problems were involved in the design and construction of this apparatus due to the high inertia loads and temperatures imposed on the test cylinder during long periods of vibration.

Test cylinders previously used in other experiments involving heat transfer from vibrating cylinders have employed guard heaters on either side of the central test section heater in order to prevent axial heat conduction away from the test section. The complexity of this arrangement -- that is, the use of three interconnecting sections, each with its own heating element and thermocouples -- has resulted in premature failure by fatigue.

In order to avoid fatigue failure, it was decided to reduce the complexity of construction of the test cylinder. This was accomplished by placing only one heater within the test cylinder. Since guard heaters were not used to prevent axial heat conduction away from the test section, a metering device was installed at each end of the cylinder to accurately measure the axial conduction heat losses to the test cylinder supports.

The test cylinder thermocouple system was designed to permit replacement of the individual thermocouples should a failure occur. A detailed description of the heat cylinder and its components is given below.

2-b. Test cylinder

The test cylinder, shown in detail in Fig. 5, consisted of a central electrically heated test section which extended between end supports that were designed to fit in the test cylinder yoke clamps. The test cylinder, 7/8" in diameter, had an overall length of 8 1/2" and weighed 1.06 lbs. The central section, called the test section, was 5.20" long.

The electric heater, installed within the test section, was made by winding gage No. 32 Nichrome V wire (nominal resistance, 10.26 ohms per foot) within a helical groove machined in the surface of a 1/2" diameter ceramic base. The helical groove had a pitch of 20 turns per inch and served to insulate the heater wire. The heater leads consisted of two pieces of 0.085" diameter drill rod which were centered at the ends of the ceramic base. The heater wires were attached to these drill rod leads with a special medium temperature solder. Regular half-and-half solder could not be used because of the high temperatures involved; silver solder was impractical because brazing temperatures in excess of 1000°F would burn the No. 32 Nichrome V heater wire. The solder used was "TEC" solder, manufactured by the Handy & Harman Brazing Products Company. This solder, composed of 5 per cent silver and 95 per cent cadmium, has a melting point of 640°F -- about 200°F above that of the available lead-tin solders.

The heater tube was closely fitted inside a copper sleeve, O.D. 5/8", and held in its axial position by Teflon plugs through which the drill rod heater leads extended as is clearly shown in Fig. 5. This assembly, with an O.D. of 5/8", was then fitted into an aluminum sleeve with an O.D. of 7/8" which was the outside element of the test section. The

copper sleeve between the ceramic heater base and the aluminum walls of the test section provided for a more uniform axial temperature distribution along the test section.

Section X-X of Fig. 5 shows the detail of the test cylinder end supports and the copper-Teflon-copper concentric rings which formed the heat meter for measuring heat loss by conduction to the test cylinder yoke supports. These concentric rings served as a heat meter in the following manner. The inner copper ring was at the temperature of the test cylinder end; similarly, the outer copper ring was at the temperature of the test cylinder yoke support. The temperature distribution along the copper rings, a length of 1 3/8", was assumed to be constant because of the excellent thermal conductivity of copper. The Teflon insulating ring produced a temperature drop between the two copper rings. This temperature differential was measured by a differential thermocouple made by soldering a gage No. 24 constantan wire between the two copper rings as shown in Section X-X, Fig. 5. The heat loss from the test cylinder by conduction to the yoke supports necessarily passed through these heat meters. This heat loss, proportional to the temperature differential, Δt_{hm}, was measured in the manner described in Chapter V.

The copper and Teflon rings were assembled on the test cylinder ends by press-fitting them firmly in place. Each heat meter thus formed a support at the test cylinder end which was held in place by the test cylinder yoke clamp. Fig. 11 provides a clear view of the final assembly.

The ends of the test cylinder were sealed by Teflon terminal plates which were fitted into each end of the aluminum sleeve a distance of

1 1/8". Small Teflon washers, 1/16" thick, separated the Teflon terminal plates and the Teflon plugs in the ends of the copper sleeve surrounding the heater tube. The outer 2 1/16" diameter flange of each terminal plate, shown in Fig. 11, was the surface on which all electrical lead connections were made. The heater lead drill rods were supported by 1/2" long stainless steel plugs which were threaded into each Teflon terminal plate. The heater lead connections from the power supply were secured to these plugs by means of special nuts through which set screws were placed so as to bear against the drill rod heater leads, thus insuring good electrical contact.

The measurement of test cylinder surface temperature was accomplished by means of thermocouples placed inside the aluminum sleeve walls. The test section was provided with six thermocouples arranged as indicated in Fig. 5 at Sections B-B through F-F. Two additional thermocouples were installed under the inner copper ring of each sandwich at Sections A-A and G-G. Thus, these two thermocouples measured the temperature of the inside copper ring within a close approximation.

The thermocouples were made of gage No. 30 dual conductor copper constantan wire encased in fiberglass insulation. Each thermocouple junction was made by removing the insulation from both wires along about 1" at the mid-span of a piece of thermocouple wire approximately 12" long. The two wires at the clean section were then twisted tightly together. Next, one end of the insulated portion of the wire was carefully pulled through a section of 0.065" diameter stainless steel tubing which had been copper-plated on its outside surface to a diameter of 0.068". When the

twisted junction was pulled just inside this tube, Handy & Harman TEC solder was used to encapsulate the junction at the tip of the tube. Each tube was then carefully fitted into its individual hole in the aluminum sleeve wall. These holes, 0.068" in diameter, received the thermocouple tubes in a tight fit; the soft copper-plating on the surface of the tubes provided excellent thermal contact between the tubes and the test cylinder wall.

The lead wires of the thermocouples and the two copper wires used for each heat meter described above were closely fitted through holes drilled in each Teflon terminal plate. From these holes the wires were led to individual terminal affixed to the terminal plate by No. 3 stainless steel screws which were threaded into the Teflon. Each wire end was formed into a spiral similar in form to the hair-spring of a watch. The spirals were secured with small copper strips held by the No. 3 screws. The spiral end prevented any wire from crossing itself and breaking from the contact when under intense vibration. The lead wires leading down the test cylinder yoke (described in Section 1-c of this chapter) were attached in a similar manner. Thus, each wire terminal consisted of spiral end from the thermocouple junction, a copper strip, the spiral end from the lead wire, a second copper strip and, finally, two No. 3 screws holding the terminal to the Teflon terminal plate. To prevent these screws from coming loose during vibration, their slots were aligned and small pieces of wire were soldered across the slots, preventing rotation of the screws.

The extreme care used in the installation and wiring of the thermocouples proved worthwhile; not one thermocouple failure occurred during the test program. However, an attractive feature of this thermocouple installation method was that an individual thermocouple could be removed and replaced in the event of failure.

The surface of the test section was polished to a mirror finish to insure a low thermal emissivity. A low value of emissivity made the radiation heat loss from the test section small compared to the heat transferred by convection. Consequently, errors made in the calculation of radiation losses did not introduce appreciable errors in the calculation of the convective heat transfer coefficient. The emissivity, as determined by comparison with a similar heat transfer test cylinder of known emissivity, was $e = 0.045$.

2-c. Power supply

The power supply to the test cylinder heater was drawn from a 500 watt constant voltage regulator. Two variacs, placed in series with the voltage regulator output, served for the coarse adjustment of the voltage across the heater. A fine adjustment was provided by a one ohm variable resistor in series with the heater. The variacs and the variable resistor were mounted on a panel together with an ammeter and voltmeter, and appropriate switches, fuses and indicator lights.

The power supplied to the test cylinder heater was measured continuously by an external Weston Model 432 double-current range wattmeter. The meter was connected in such a manner that the meter indication

included only its potential circuit losses. On low scale, used to measure power below 30 watts, the internal resistance of the potential circuit was 4083 ohms, as measured by a high precision portable wheatstone bridge. On high scale, used to measure power above 30 watts, this resistance was 8180 ohms. The resistance of the heater was 90.07 ohms; the resistance of the heater leads was 0.17 ohms. Thus, with the meter on low scale, the potential and lead circuit loss was 2.16 per cent of the wattmeter indication; on high scale the loss was 1.09 per cent of the wattmeter indication.

2-d. Temperature measuring apparatus

The eight thermocouples mounted in the test cylinder walls and the two additional thermocouples used to measure ambient temperature in the test room were connected through a Minneapolis-Honeywell thermocouple selector switch to a common cold junction and a portable Rubicon precision potentiometer. The cold junction was placed in a thermos bottle filled with water and ice.

The differential thermocouples of the two heat meters at the test cylinder ends were connected to the Rubicon precision potentiometer through a double-pole, double-throw knife switch. The thermocouple selector switch was put on open circuit when it was desired to obtain the heat meter temperature differential at each end of the test cylinder.

Standard tables were used to convert the potentiometer readings to temperatures. It was considered that errors associated with determining absolute temperatures and temperature differences with this system were within $0.1^{\circ}F$.

CHAPTER IV

EXPERIMENTAL PROCEDURE

The experimental program was carried out in two phases. The first phase, called the calibration phase, was a series of tests performed with no vibration in order to determine the heat loss by conduction, Q_d, to the test cylinder supports. The second phase, called the vibration phase, involved the collection of heat transfer data with the test cylinder in horizontal vibration.

The calibration phase was carried out with the test stand and test cylinder in the horizontal position as shown in the photograph, Fig. 10. The test section heat input was set at integral multiples of 5 watts from 5 to 50 watts. Two additional tests were conducted at wattmeter settings of 60 and 70 watts. The rated accuracy of the wattmeter was 0.5 per cent of full scale deflection; hence, the maximum possible error of the wattmeter reading occurred at the 5 watt level and was 3.5 per cent. The possible error at the 70 watt level was 0.54 per cent.

Since the heat input to the test cylinder was kept constant during a given test, the steady state temperatures of the test cylinder were approached exponentially in time. The criterion established for terminating the calibration phase tests was a maximum change in any individual test cylinder thermocouple reading of $0.2^{\circ}F$ and a maximum change in heat meter temperature differential, Δt_{hm}, of $0.1^{\circ}F$ over a period of one-half hour. In practice, a steady state temperature was generally achieved with less variation than the above requirements. The average calibration test run extended for a period of approximately four hours.

The ambient temperature, t_a, was given by a thermocouple placed about 15" below the test section. A second thermocouple, suspended in the test room about 3 ft above and behind the test cylinder was monitored, and generally read within $0.2^{\circ}F$ of the thermocouple below the test section.

The surface temperature of the test section was defined as the average of the six temperature readings from the six thermocouples in the test section locations indicated in Chapter III, Section 2-b. As expected, the axial distribution of the individual test section temperature readings showed a variation dependent on heater power level. The variation between the center and end individual test section temperatures ranged from $4.0^{\circ}F$ at the 5 watt level to $40.3^{\circ}F$ at the 70 watt level. The temperature potential, Δt, based on average surface temperature, t_s, from the six test section thermocouple readings was $25.6^{\circ}F$ for the 5 watt level and $273.9^{\circ}F$ for the 70 watt level. Thus, considering the worst condition - that the average t_s was in error by one-half of the axial temperature range ($2^{\circ}F$ for the 5 watt case and $20.15^{\circ}F$ for the 70 watt case) - the percentage error in Δt would be 7.81 per cent at the 5 watt level and 7.38 per cent at the 70 watt level. These errors, of course, represent the unlikely extreme; in actual test, the measured average test cylinder surface temperature was estimated to be within 2 per cent of the true mean surface temperature.

The temperature differential across the heat meters at the test cylinder supports was provided by the differential thermocouples (described in Chapter III, Section 2-b). The temperature level from which the temperature differential was measured was provided by the thermocouple

immediately beneath each heat meter in the test cylinder surface (at Sections A-A and G-G, Fig. 5). The left and right heat meter temperature differentials were always within $2^{o}F$ of each other. This variation was due to a small difference in heat flow across the left and right test cylinder heat meters. In practice, the average of the two heat meter temperature differentials was taken as the test cylinder end temperature difference, Δt_{hm}. As stated in Chapter III, Section 2-d, it was considered that the errors associated with determining absolute temperatures and temperature differences with this system were within $\pm 0.1^{o}F$.

The results of twelve calibration phase test runs are given in Table 1 and plotted in Fig. 13. The method used in calculating these results is presented in Chapter VI.

The vibration phase of the experimental program was oriented toward the major objective of the entire investigation; namely, the investigation of the influence of horizontal mechanically induced simple harmonic vibrations upon the heat-transfer rate by free convection from a heated horizontal cylinder to air. Specifically, the tests were so arranged as to provide data which could be compared directly with the sound method data obtained by Fand and Kaye as explained in Chapter I.

The three principal experimental variables were as follows:

a. temperature potential, Δt

b. intensity of vibration, af

c. heat input to the heat transfer cylinder test section, Q_w

In order to provide a direct comparison with the sound method experiments of Fand and Kaye in a small number of test runs, it was decided to restrict

the independent variable Δt to one value, namely, $\Delta t = 150^{\circ}F$. Since, in practice, it would be extremely difficult to obtain an exact steady state value of $\Delta t = 150^{\circ}F$ for each test, the allowable variation from this temperature potential was established as $\pm$ 1.0°F. It was also necessary to vary af within a range of about 0.2 to 1.1 ft/sec to cover the same range of vibration intensity as was done in the sound method experiments.

The vibration tests were all made at the same frequency, f = 104 cps, the resonant frequency of the mechanical system. At the start of each test, the vibration exciter was tuned to this resonant frequency. Tuning was achieved by applying the principle that for a coupled electro-mechanical system with a constant electrical energy input, the current becomes a minimum at resonance. An additional aid in determining resonance was the fact that the maximum apparatus noise level, while not large, coincided with the resonant condition.

After obtaining vibration at resonance, the desired value of af was acquired by adjusting the output level of either the audio-oscillator or its amplifier or both. Also, at lower vibration intensities it was found convenient to limit the value of the direct current output to the exciter field coil to an arbitrary value less than the 1.75 ampere rating. This procedure, in effect, added sensitivity to the gain controls of the audio-oscillator and amplifier and thereby aided in establishing the desired amplitude. These gain controls were adjusted in trial and error fashion until the double amplitude of vibration was at the value required to give the proper af value for the test run. This procedure, initially

tedious, was usually accomplished within 10 minutes after some experience had been acquired. The vibration amplitude was checked at 5 minute intervals; minor correction was occasionally necessary.

The requirement of producing a steady state value of Δt within $1^{\circ}F$ of $150^{\circ}F$ was more difficult to achieve. Because the steady state heat input to the test cylinder with vibration was unknown, its value had to be determined in each test run. The power supplied to the test section which resulted in a $150^{\circ}F$ temperature potential in the absence of vibrations was determined to be about 34 watts from the results of the calibration tests. It was assumed that the power level needed to produce the same temperature potential with the test cylinder in vibration was greater. The test cylinder was heated for about two hours prior to vibration at a power level somewhat greater than 34 watts. After the desired vibration intensity was established, a complete set of temperature readings was taken at 10 minute intervals. The temperature potential existing at the time of temperature measurement was then quickly computed, and the power level was adjusted to bring Δt closer to $150^{\circ}F$. This process was repeated until no change in Δt greater than $0.1^{\circ}F$ in a 10 minute period was detected. At this time the watt meter reading was recorded as the steady state value, and the cathetometer readings of vibration amplitude were recorded.

The duration of the individual vibration tests varied between two and three hours. The results of the nine tests with vibration are recorded in Table 2 and plotted in Fig. 14. The method used in calculating these results is presented in Chapter V.

CHAPTER V

CALCULATION PROCEDURE AND RESULTS

This chapter contains a description of the methods and basic calculation procedure used to evaluate and interpret the experimental data, and a description of the results obtained.

The calibration phase tests of the experimental procedure provided data with which the axial heat losses from the test cylinder could be determined as a function of average heat meter temperature differential, Δt_{hm}. During the tests in the absence of vibration, the heat input to the test section, Q_w, was dissipated to the system environment by the following modes of heat transmission:

a. Heat loss from the test section by radiation, Q_r

b. Heat loss from the test section by convection (in the absence of vibration), Q_{co}

c. Heat loss to the test cylinder supports, Q_d

d. Heat loss by convection from the end terminal plates of the test cylinder and heat loss by conduction through the test cylinder lead wires (in the absence of vibration), Q_{uo}, called the unaccountable heat loss.

The test section heat losses by radiation and convection, Q_r and Q_{co}, were subject to accurate calculation as will be described below. Calculation of the heat loss to the test cylinder supports, Q_d, could not be accurately calculated, however, because: (1) the thermal conductivity of the heat meter Teflon ring was not known within the required accuracy,

and (2) the contact coefficient of the copper-Teflon heat meter junctions -- a function of test cylinder support clamping pressure, surface roughness and the presence of oxide films -- could not be determined. Further, calculations for Q_d, using the best available value of thermal conductivity for Teflon, gave results that did not agree well with the empirical determination of Q_d as described below. Similarly, Q_{uo} could not be calculated because of the complicated geometry of the outside surface of the Teflon plates.

The sum, $(Q_d + Q_{uo})$, could be determined, however, through application of the following heat flow continuity equation:

$$Q_d + Q_{uo} = Q_w - (Q_r + Q_{co}) \qquad (6)$$

In the calibration phase tests, $(Q_d + Q_{uo})$ was determined as a function of Δt_{hm}. The results of these tests are plotted in Fig. 13. The original experimental data for the calibration tests and the associated calculated quantities are listed in Table 1. The experimentally determined curve of $(Q_d + Q_{uo})$ versus Δt_{hm} is very nearly a straight line which indicates that the predominate heat loss at the test cylinder ends was by conduction, i.e., $Q_d + Q_{uo}$. This was the expected result since the outside surface temperature of the Teflon terminal plates was much less than the temperature of the test cylinder. Also, the heat loss by conduction through the lead wires was negligible compared to Q_d.

The heat transferred by convection in the presence of vibrations, Q_{cv}, was determined from the heat continuity equation:

$$Q_{cv} = Q_w - Q_r - (Q_d + Q_{uv}) \qquad (7)$$

where Q_{uv} is the unaccountable heat loss in the presence of vibration. It is recognized that Q_{uv} was somewhat greater than Q_{uo} due to the increase in convective heat transfer from the terminal plates in the presence of vibrations; however, this difference, $(Q_{uv} - Q_{uo})$ was assumed negligible since the unaccountable heat loss itself was small. Accordingly, in the tests with vibration, Q_{cv} was computed by:

$$Q_{cv} = Q_w - Q_r - (Q_d + Q_{uo}) \tag{8}$$

where $(Q_d + Q_{uo})$ was determined from Fig. 13.

The heat transferred by convection from the test section in the absence of vibration, Q_{co}, was determined in the following manner. The defining equation of the heat-transfer coefficient in the absence of vibration, h_o, is:

$$h_o = 3.412 \frac{Q_{co}}{A \Delta t}, \text{ Btu/hr-ft}^2\text{-}^o\text{F} \tag{9}$$

where

A = test section heat transfer area, 0.0993 ft^2

Q_{co} = heat transferred by convection, watts

Δt = temperature potential, ^{o}F

3.412 is the conversion factor from watts to Btu/hr

The experimentally determined equation[9] for h_o of a cylinder of diameter D_o is:

$$h_o = 0.225 \left(\frac{\Delta t}{D_o}\right)^{1/4}, \text{ Btu/hr-ft}^2\text{-}^o\text{F} \tag{10}$$

Equation (10) was the result of a heat-transfer study with a cylinder of identical diameter (7/8"), length and end support method and surface thermal emissivity as the test cylinder used in this project.

Equating Equations (9) and (10) with $D_o = 0.0729$ ft and solving for Q_{co} gives:

$$Q_{co} = 0.0143 \, \Delta t^{5/4} \text{ , watts} \qquad (11)$$

The maximum experimental error in the determination of h_o by Equation (10) was reported to be 2.6 per cent.[9] The maximum possible experimental error in the calculated value of Q_{co} was determined by logarithmic differentiation of Equation (9):

$$\frac{dh_o}{h_o} = \frac{dQ_{co}}{Q_{co}} - \frac{dA}{A} - \frac{d(\Delta t)}{\Delta t} \qquad (12)$$

Equation (12) was written in finite difference form; hence, the maximum possible percentage error in Q_{co} was the sum of the maximum possible percentage errors of the quantities involved in its calculation. The possible error in h_o was 2.6 per cent; the possible error in the calculation of surface area, A, was less than 0.2 per cent. The maximum error in Δt was estimated to be 2 per cent (see Chapter IV). Thus, the maximum possible error in the value of Q_{co} was 4.8 per cent.

The heat transferred by radiation from the test section, Q_r, was independent of the presence of vibrations. Q_r, as a function of Δt, was determined from the graph, Fig. 12, based on the equation:

$$Q_r = 0.2931 \, \sigma e A \left[(t_b + t)^4 - t_b^4 \right] \text{ , watts} \qquad (13)$$

where

σ = Stefan-Boltzman constant, 0.1713×10^{-8} Btu/ft^2-hr-$^\circ$R^4

e = surface thermal emissivity of the test section, 0.045

A = test section heat transfer area, 0.0993 ft^2

t_b = mean ambient temperature, 540°R

Δt = temperature potential, $^\circ$F

0.2931 = conversion factor from Btu/hr to watts

The errors associated with determining Q_r, which were introduced by the fact that the actual ambient temperature was in most cases slightly different from the mean ambient temperature, were less than 4 per cent. These errors were negligible because Q_r itself was small compared to the total heat transferred from the test section.

The heat transfer coefficient in the presence of vibration, h_v, was calculated for each test of the vibration phase by using the heat transferred by convection, Q_{cv}, for the test as determined by Equation (8). Thus:

$$h_v = 3.412 \frac{Q_{cv}}{A \Delta t}, \text{ watts} \qquad (14)$$

The maximum possible experimental error in the calculated value of h_v was determined by writing the logarithmic differential equation of (14) in finite difference form as in the case for Q_{co} above. The maximum possible error involved in obtaining Q_{cv} was 3.0 per cent, as obtained by adding the maximum errors possible in Q_w and $(Q_d + Q_{uo})$. Errors in Q_r were less than 0.1 per cent and were neglected. Again the errors in surface area, A, and Δt were taken as 0.2 and 2 per cent, respectively.

Thus, the maximum possible experimental error in the determined value of h_v was 5.2 per cent.

The experimental data and the calculated results of nine tests with vibration are recorded in Table 2. The range of vibration intensity employed was from 0.213 to 1.109 ft/sec; the temperature potential in all these tests was within $\pm$ 1°F of 150°F. The value of h_v varied from 1.803 Btu/hr-ft^2-°F at the lowest af to 4.323 Btu/hr-ft^2-°F at the highest af. The value of h_o at Δt = 150°F was computed to be 1.717 Btu/hr-ft^2-°F by Equation (10). Thus, percentage increases in the heat-transfer coefficient from 5.0 to 151.8 per cent were achieved.

In order to provide a direct comparison of these results with the sound method investigation of Fand and Kaye[10] (discussed in Chapter I), the variation of h_v with af at Δt = 150°F for a stationary horizontal cylinder in the presence of a high intensity sound field of frequency f = 1496 cps was obtained from Fig. 61 of Reference 10 by cross-plotting. The data points of the vibration tests of the present investigation were then plotted on the same graph, Fig. 14. The maximum deviation of any single data point from the sound method curve in Fig. 14 is 4.6 per cent as compared to the maximum possible experimental error of 5.2 per cent in obtaining the data points. Fand and Kaye arrived at a correlation equation which expressed the dependence of h_v on Δt and af with a high degree of consistency above an af of about 0.7 for sound frequencies less than 2000 cps. For convenience, this correlation equation is restated here:

$$h_v = 0.722 \left[\Delta t \, (af)^2 \right]^{1/3} \qquad (1)$$

The maximum deviation of h_v obtained in this investigation for the three values of af greater than 0.7 from the computed value h_v given by Equation (1) was 7.3 per cent. The average deviation was 2.1 per cent.

A comparison of the results of this investigation with the results of the study of heat-transfer rate variation with vertical mechanical vibrations[8] (discussed in Chapter I) was also made. A curve of h_v versus af for $\Delta t = 150^{\circ}F$ was obtained from Fig. 12 of Reference 8 and is plotted in Fig. 15 of the present report. The data points of the vibration phase of this investigation were plotted on Fig. 15 to facilitate comparison. Inspection of Fig. 15 revealed that the trend of h_v increase relative to af was quite similar for the two investigations. In particular, at values of af above about 0.3 ft/sec, the value of h_v is somewhat less for the horizontal vibration case, while the slopes correspond closely. This result will be discussed further in Chapter VI.

It was considered desirable to obtain some visual evidence of the type of boundary-layer flow that existed around the heated test cylinder during vibration. Accordingly, a crude flow-visualization examination was performed, using a lighted cigarette held beneath the cylinder as a smoke source. The results of this visual observation clearly indicated that laminar flow persisted in the region near the lower stagnation point throughout a range of af from 0 to about 1.1 ft/sec. Also, some evidence of vortex formation above the cylinder was noted; this vortex flow is characteristic of thermoacoustic streaming as observed by Fand and Kaye in their sound studies. Although the results of the elementary visualization technique employed here require further substantiation, the study

did indicate conclusively that the fluid flow mechanism in the region of the lower stagnation point of the cylinder was not vibrationally induced turbulence as reported for the vertical vibrations case[8, 9].

CHAPTER VI

DISCUSSION OF RESULTS

The results of the present experimental investigation reaffirm the conclusions of previous investigations that the influence of vibrations on heat transfer is significant. The plots of h_v versus af (Figs. 14 and 15) clearly indicate the general effect of the intensity of vibration on the heat-transfer rate from a heated horizontal cylinder in horizontal transverse vibration in air. It was noted that the change in h_v at vibration intensities less than af = 0.3 ft/sec is not appreciable. Above this value of vibration intensity, the heat-transfer coefficient increases rapidly with increasing af. The value of af = 0.3 ft/sec, where vibrations take on major significance with regard to the heat-transfer rate is called the critical intensity. The critical intensity, af = 0.3 ft/sec, observed in this investigation corresponds very nearly to the critical intensities reported for the sound method (Fig. 14) and also in the vertical mechanical vibrations method (Fig. 15).

The close agreement of the quantitative heat transfer results and the flow visualization observations of this investigation with those of the sound method for comparable vibration vector orientation provides evidence which indicates that the physical mechanism of the heat transfer for the two cases is identical. However, the quantitative results, when compared to the vertical vibrations method (Fig. 15), show that the slopes of h_v versus af are very nearly the same for these two cases. The fact that the trend of the data obtained in this investigation is similar

to the results of the vertical vibrations method (Fig. 15) is not considered evidence that the two modes of vibration are equivalent with respect to heat transfer; for, as has been explained in Chapter V, the mechanism of interaction between vibrations and free convection in the case of vertical vibration is vibrationally induced turbulence, whereas there is evidence that the mechanism of interaction for both the sound method and the present investigation is thermoacoustic streaming.

The slope of h_v versus af for af greater than about 0.9 for the sound method is 2/3 as Equation (1) indicates. The corresponding slope for the vertical vibrations method has been reported to be 1[9]. Additional heat transfer data is required for values of af greater than 0.9 to determine conclusively the value of this slope for the horizontal vibrations method.

The ratio of amplitude of vibration to cylinder diameter, a/D_o, is a controlling variable in all fluid-mechanical phenomena involving vibrations. The a/D_o ratio for this investigation at a typical value of af = 0.9 ft/sec and f = 104 cps was 0.119; the a/D_o ratio for the sound method of Fand and Kaye with af = 0.9 ft/sec at f = 1496 cps was 9.63×10^{-3}. Thus, the a/D_o ratios differed by a factor of 12.3. In view of the close quantitative agreement of the results of the two methods of investigation (Fig. 14), it appears that the influence of a/D_o does not have a predominant effect, at least for the range of a/D_o ratios indicated here.

CHAPTER VII

CONCLUSIONS

The experimental portion of this investigation of the influence of horizontal mechanically induced vibrations on the heat-transfer rate from a horizontal cylinder to air consisted of a total of 21 heat transfer test runs. Twelve of these test runs provided calibration data on axial heat loss from the heat transfer test cylinder; nine test runs were conducted with the cylinder in horizontal vibration. The ranges of the principal experimental variables were:

temperature potential, Δt:	$150^{\circ}F \pm 1^{\circ}F$
frequency of vibration, f:	104 cps
amplitude of vibration, a:	0.025 to 0.128"
intensity of vibration, af:	0.21 to 1.11 ft/sec

The results indicate that the influence of horizontal vibrations upon the heat-transfer rate by free convection to air becomes appreciable when the intensity of vibration, defined as the product af, exceeds the critical value of 0.3 ft/sec. This critical value is approximately equal to the critical sound vibration intensity determined in Reference 10 and the critical value of af for vertical mechanical vibrations determined in Reference 9. The flow near the horizontal cylinder in the presence of intense mechanically induced transverse horizontal vibrations was observed to be laminar near the lower stagnation point using smoke as the indicating medium; this type of flow is one characteristic of the flow

near the lower stagnation point of a cylinder in the presence of intense acoustically induced transverse horizontal vibrations. The observed laminar flow near the lower stagnation point was quite different from the vibrationally induced turbulent flow characteristic of horizontal cylinders in transverse vertical vibration.

Based on the quantitative heat transfer results and the elementary flow study of this investigation, it appears that the physical mechanism of heat transfer for the sound and mechanical vibrations methods, both with geometry as indicated in Fig. 1-a, is identical. Also, the comparison of these two methods indicates that the amplitude of vibration to cylinder diameter ratio, a/D_o, does not have a predominant effect for the range of a/D_o ratios considered.

CHAPTER VIII

RECOMMENDATIONS

This chapter presents recommendations for future investigations in the field of heat transfer from vibrating cylinders based on the results and experience gained from the present project. Six specific suggestions are made; the first five of these relate to experimental work that can be conducted with the apparatus designed and constructed for this project. Indeed, this apparatus was designed to include features whereby adaptation to other investigations will require minor or no modification. The list of suggested investigations with a few relevant remarks is given below.

(1) Extension of the range of vibration intensity to values of af greater than 1.1 ft/sec. This is necessary, as indicated in Chapter VI, in order to determine accurately the slope of h_v versus af in the higher af range. The existing apparatus has been tested at af = 1.3 ft/sec with about 35 lbs exciter driving force. It is considered that an af of at least 1.5 ft/sec can be achieved at the maximum exciter output of 50 lbs force.

(2) Flow visualization studies. It would be of particular value to obtain photographic evidence of the flow pattern around the test cylinder.

(3) Change in vibration direction relative to the direction of the force of gravity. Since the flow character around the cylinder has been shown to be different for the vertical and horizontal vibration cases, it would be of value to investigate vibration angles between these two extremes. This can be done with the existing apparatus as described in Chapter III, Section 1.

(4) An investigation of velocity and temperature distributions near the cylinder. It is considered that hot-wire anemometry techniques could be used to determine detailed information concerning the heat transfer mechanism near the cylinder by an investigation of this type.

(5) Different cylinder diameters. The quantitative determination of the influence of cylinder diameter is important. New test cylinders and some modification of the test cylinder yoke would be required.

(6) Analysis. It is considered that, on the basis of the data provided herein and from other investigations in the field, an analysis should be attempted which would provide a mathematical foundation for the phenomena observed.

F I G U R E S

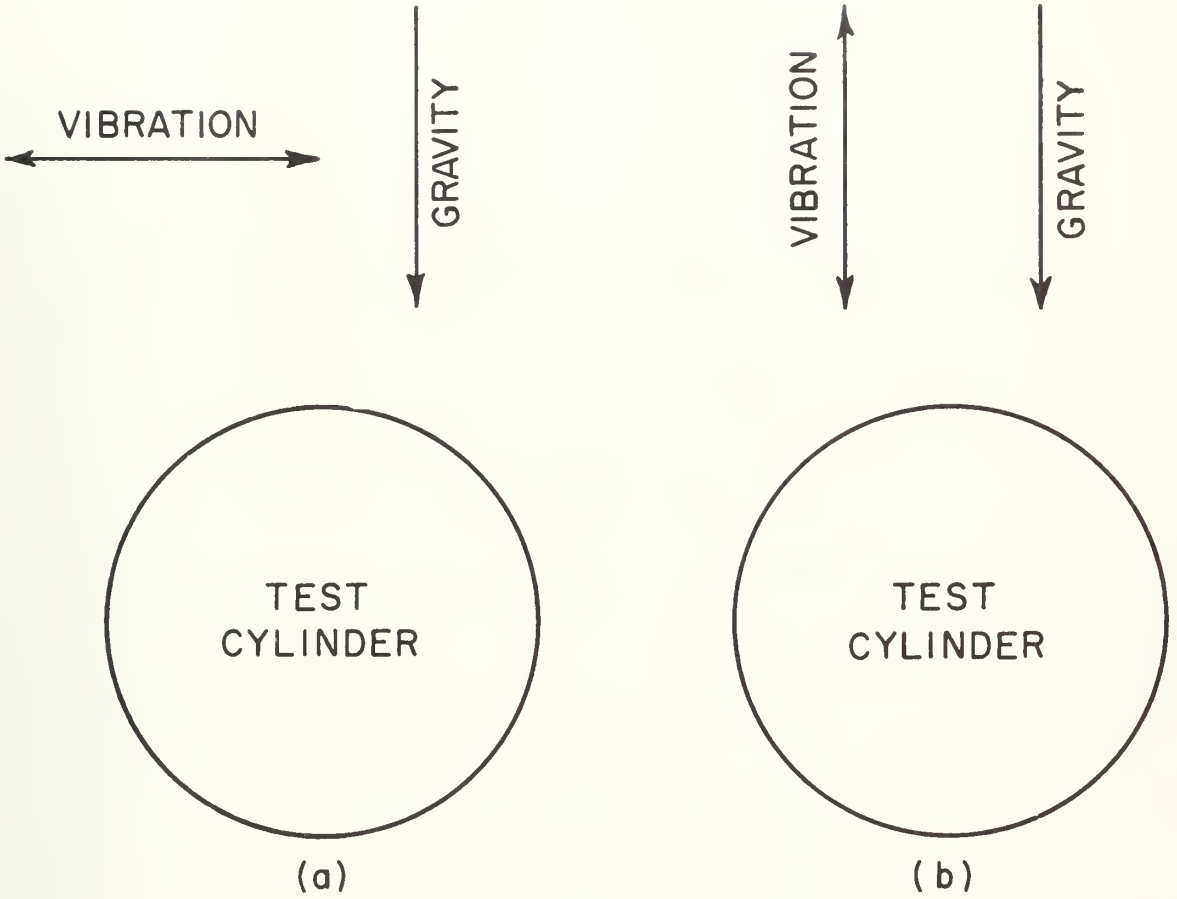

FIG. 1 ORIENTATION OF VIBRATION VECTOR RELATIVE TO DIRECTION OF GRAVITY FOR (a) HORIZONTAL TRANSVERSE VIBRATIONS AND (b) VERTICAL VIBRATIONS OF A HORIZONTAL CYLINDER

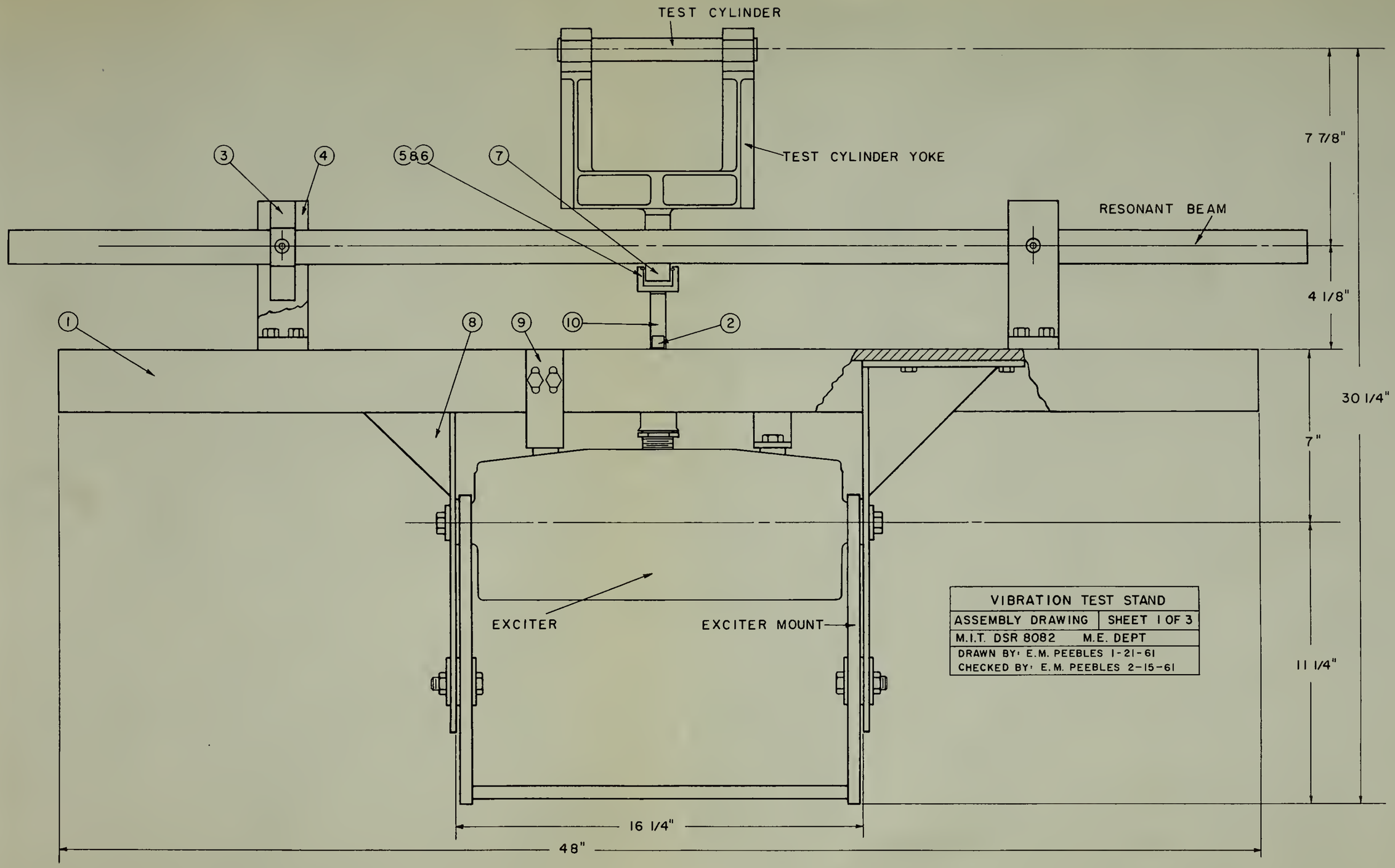
TEST CYLINDER
TEST CYLINDER YOKE
RESONANT BEAM
3
4
5&6
7
1
8
9
10
2
7 7/8"
4 1/8"
30 1/4"
7"
11 1/4"
EXCITER
EXCITER MOUNT
16 1/4"
48"
VIBRATION TEST STAND
ASSEMBLY DRAWING
SHEET 1 OF 3
M.I.T. DSR 8082
M.E. DEPT
DRAWN BY: E.M. PEEBLES 1-21-61
CHECKED BY: E.M. PEEBLES 2-15-61

Fig. 2

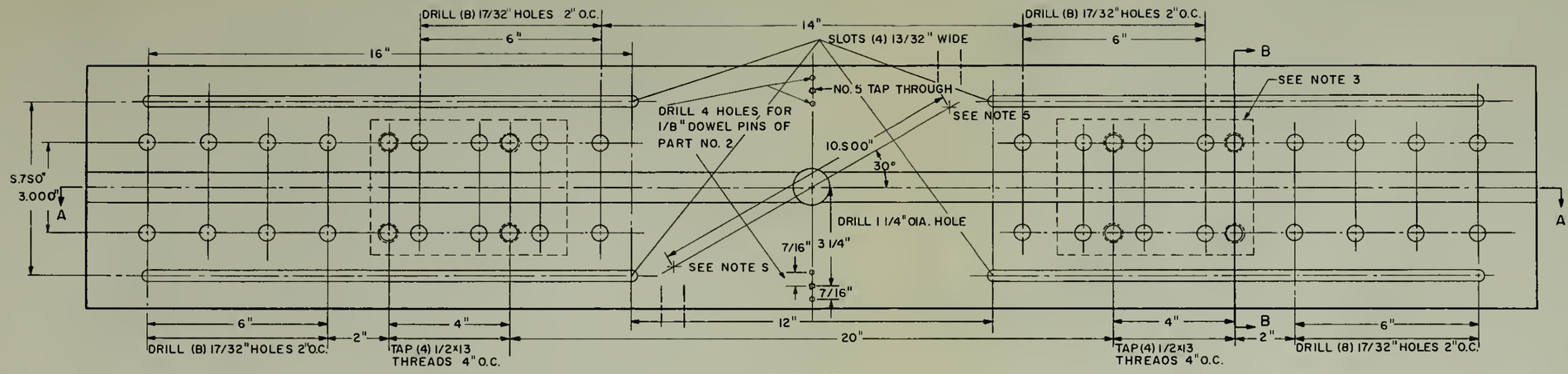

TOP VIEW

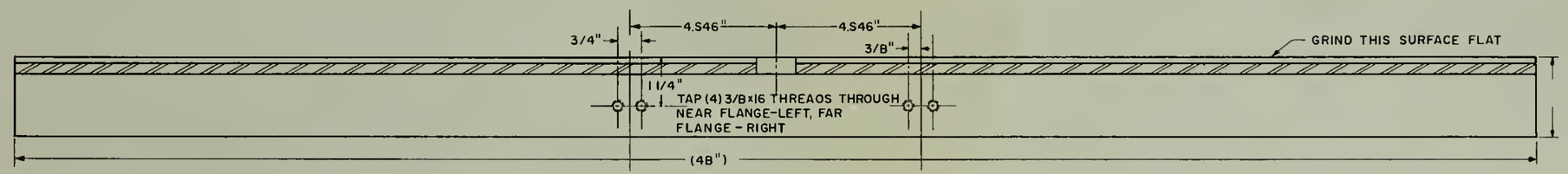

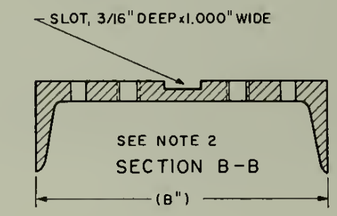

SECTION A-A

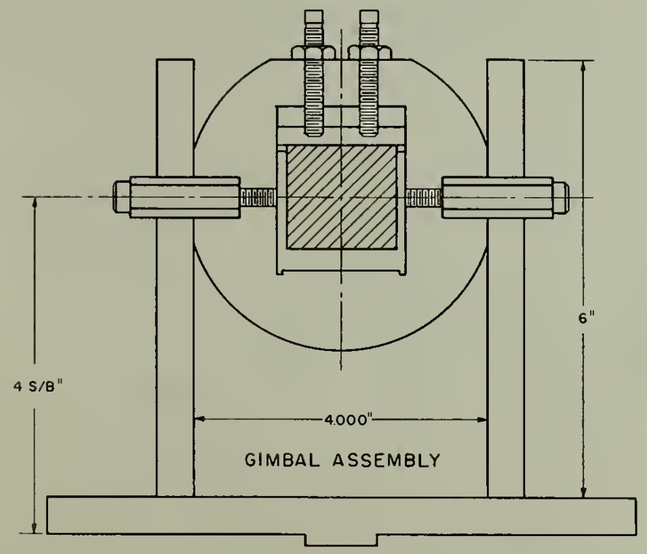

1 ALIGNMENT PLATFORM

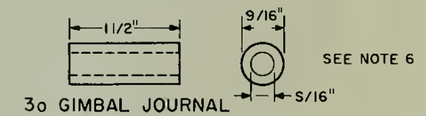

3a GIMBAL JOURNAL

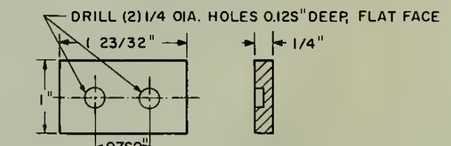

3b BEAM CLAMP PLATE

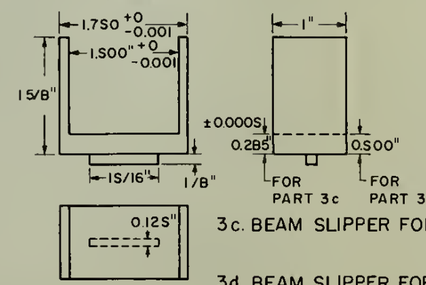

3c. BEAM SLIPPER FOR 1.43x1.50 BEAM

3d. BEAM SLIPPER FOR 1.00x1.50 BEAM

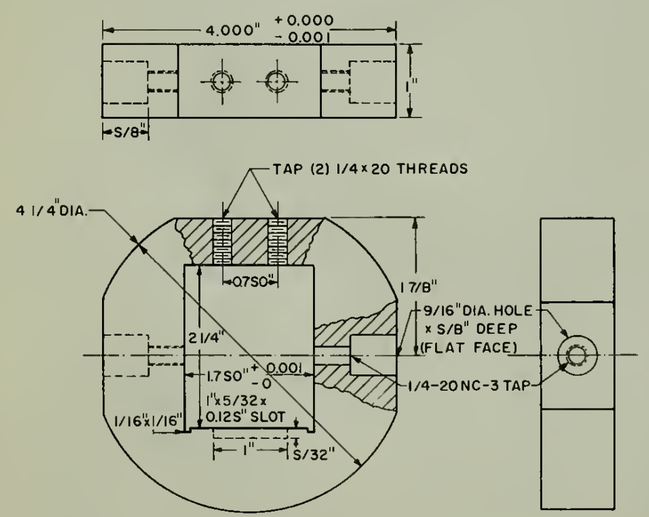

3e GIMBAL FRAME

NOTES:

1. DIMENSIONS IN BRACKETS INDICATE NOMINAL SIZE OF MATERIAL, AS DELIVERED.
2. GRIND BOTTOM 5/16" EITHER SIDE OF SLOT ℄ ALONG LENGTH OF SLOT.
3. INDICATES POSITION OF QUADRANT SUPPORT PLATE CONTACT ON CHANNEL BOTTOM. GRIND THIS AREA FLAT.
4. DRILL DOWEL PIN HOLES IN PARTS 1 & 2 AT THE SAME TIME.
5. DEFINES LOCATION (UNDER) OF SPOT FACE TAPS ON EXCITER CASTING TOP AND THE LENGTH-WISE DIMENSION FROM WHICH THE 4 FLANGE TAPS SHOULD BE LOCATED.
6. PART 3a TO HAVE LIGHT PRESS FIT INTO PART 3e & SLIDING FIT THROUGH PART 4.

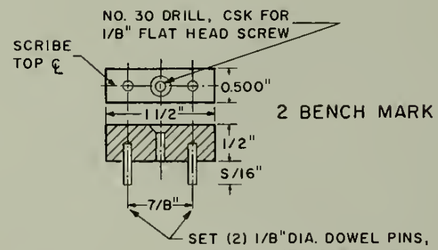

2 BENCH MARK

DESCRIPTION OF PART	NO. REQ'D	MATERIAL	REMARKS
1. ALIGNMENT PLATFORM	1	STRUCTURAL STL	8 WIB.S 4'-0"
2. BENCH MARK	2	303 STAINLESS	
3a. GIMBAL JOURNAL	4	1020 ST. H.R.	
3b. BEAM CLAMP PLATE	2	303 STAINLESS	
3c. BEAM SLIPPER	2	303 STAINLESS	FOR 1.43x1.50 BEAM
3d. BEAM SLIPPER	2	303 STAINLESS	FOR 1.00x1.50 BEAM
3e. GIMBAL FRAME	2	2024-T4 AL.	
VIBRATION TEST STAND			
DETAIL DRAWINGS OF PART 1, 2 & 3			SHEET 2 OF 3

Fig. 3

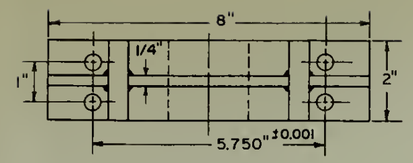

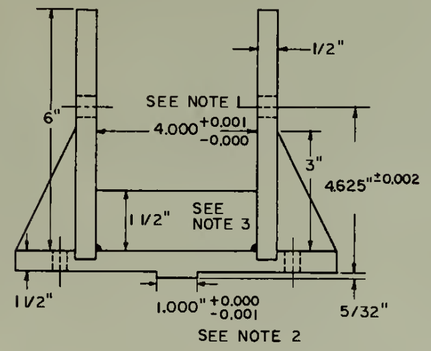

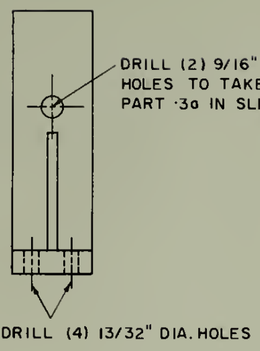

4 GIMBAL SUPPORT

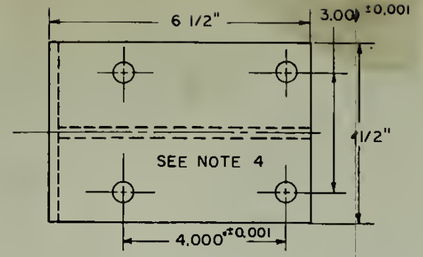

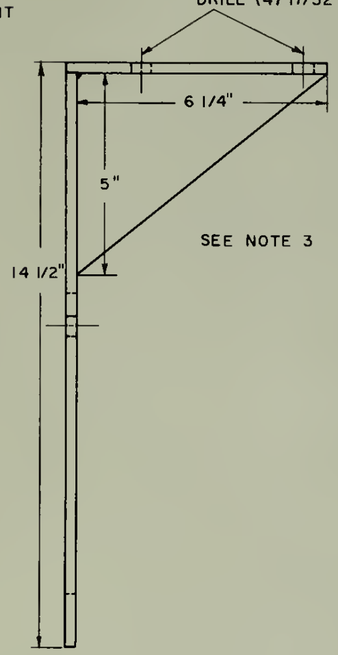

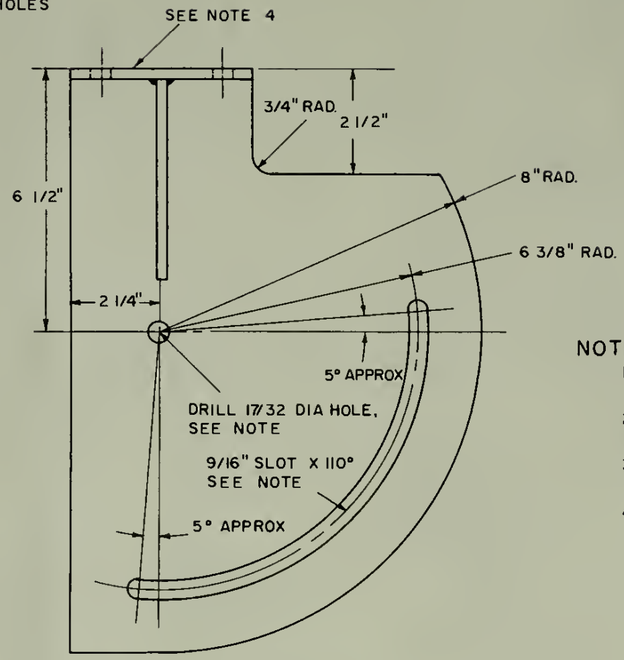

8 QUADRANT

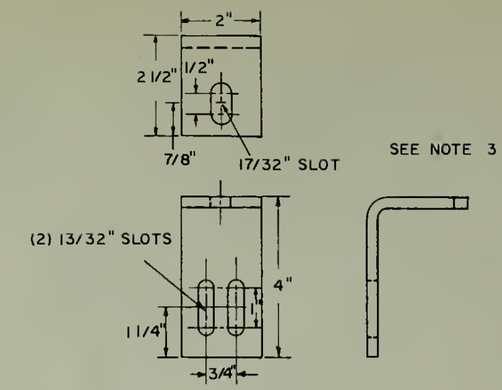

9 BRACKET

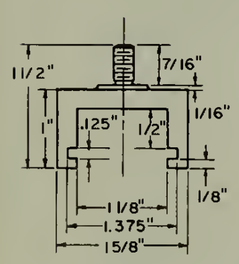

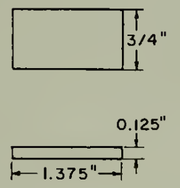

6 LOAD PLATE

5 LOAD PLATE YOKE

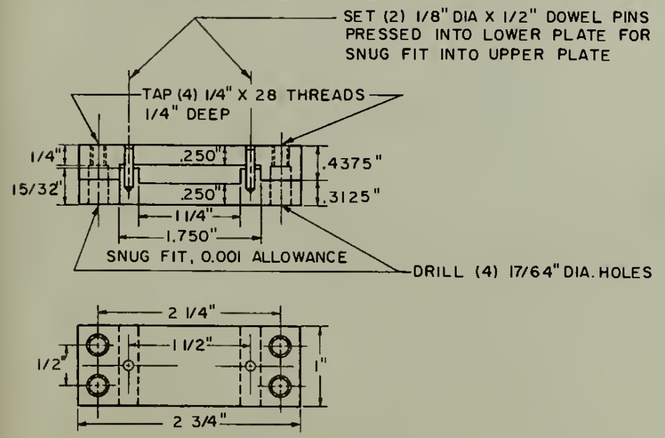

7 CLAMPING PLATE ASS'Y

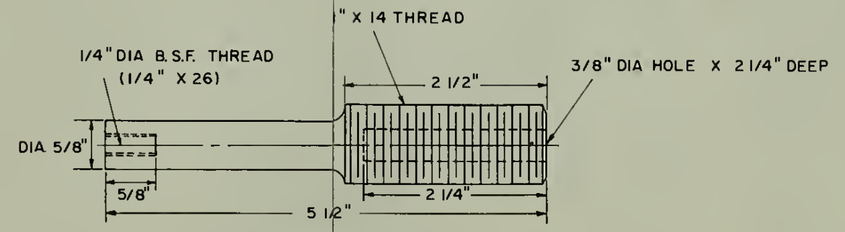

10 EXCITER EXTENSION

NOTES

1. PART 4. PART 3 TO FIT WITHIN POSTS WITH 0.001" MAX. CLEARANCE
2. PART 4. PAD PROJECTION TO HAVE CLOSE, SLIDING FIT WITHIN SLOT OF PART 1
3. PTS 3 & 8. COMPLETE ALL WELDING BEFORE DRILLING & MACHINING
4. GRIND LOAD SURFACE FLAT WITH THE 2 QUADRANTS FIXED BACK-TO-BACK

DESCRIPTION OF PART	NO. REQ'D	MATERIAL	REMARKS
4. GIMBAL SUPPORT	2	304 STAINLESS	1/2" STOCK
5. LOAD PLATE YOKE	1	1020 ST. H.R.	5/8" X 1 1/2" RECT. ROD
6. LOAD PLATE	1	RY-ALLOY	5/32" X 3/4" GROUND STOCK
7. CLAMPING PLATE ASS'Y	1	1020 ST. H.R.	
8. QUADRANT	2	MILD STEEL	1/4" PLATE
9. BRACKET	2	MILD STEEL	1/4" PLATE
10. EXCITER EXTENSION	1	AL. 2024-T4	

VIBRATION TEST STAND

DETAIL DRAWING OF PARTS 4-10 | SHEET 3 OF 3

Fig. 4

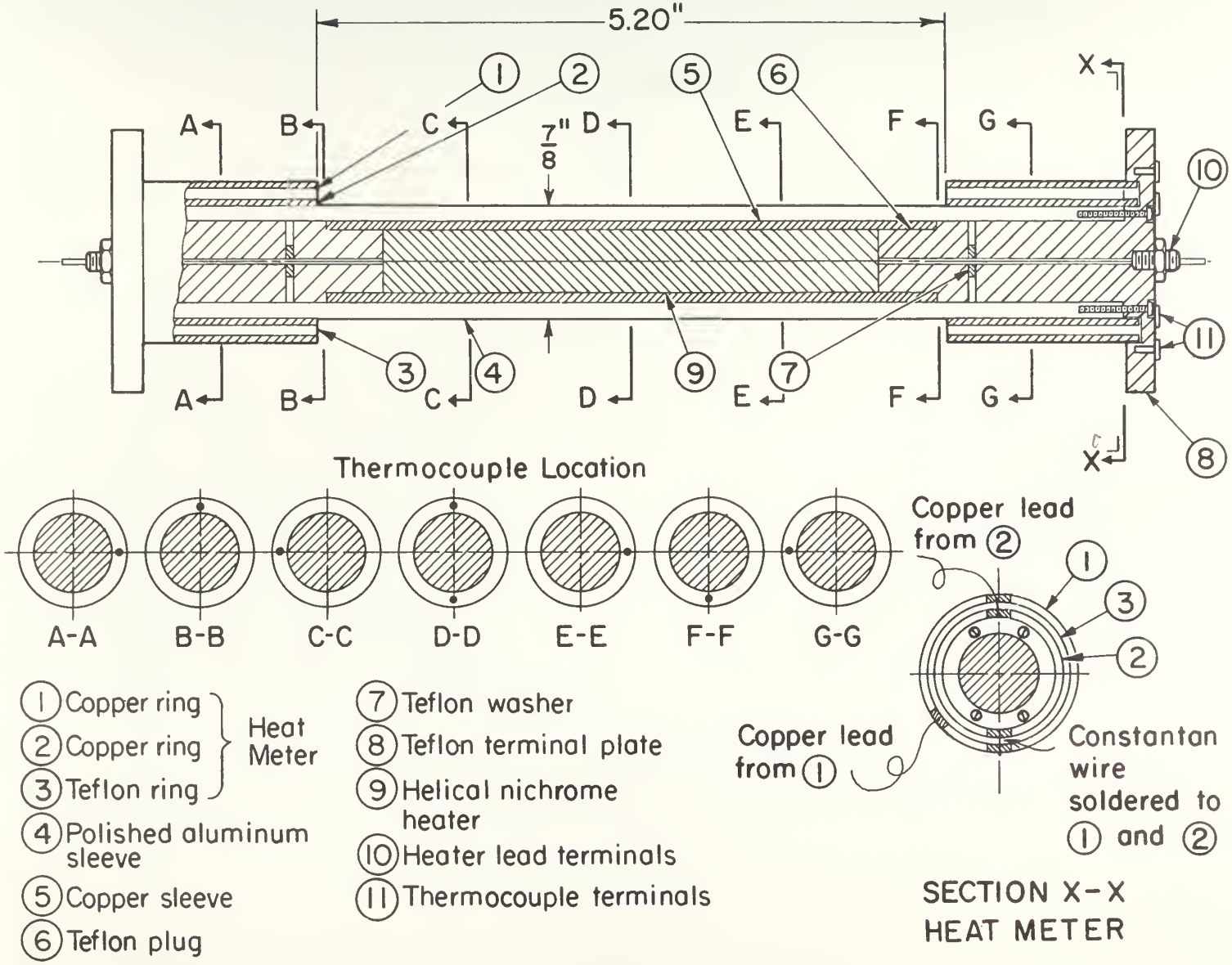

FIG. 5 TEST CYLINDER

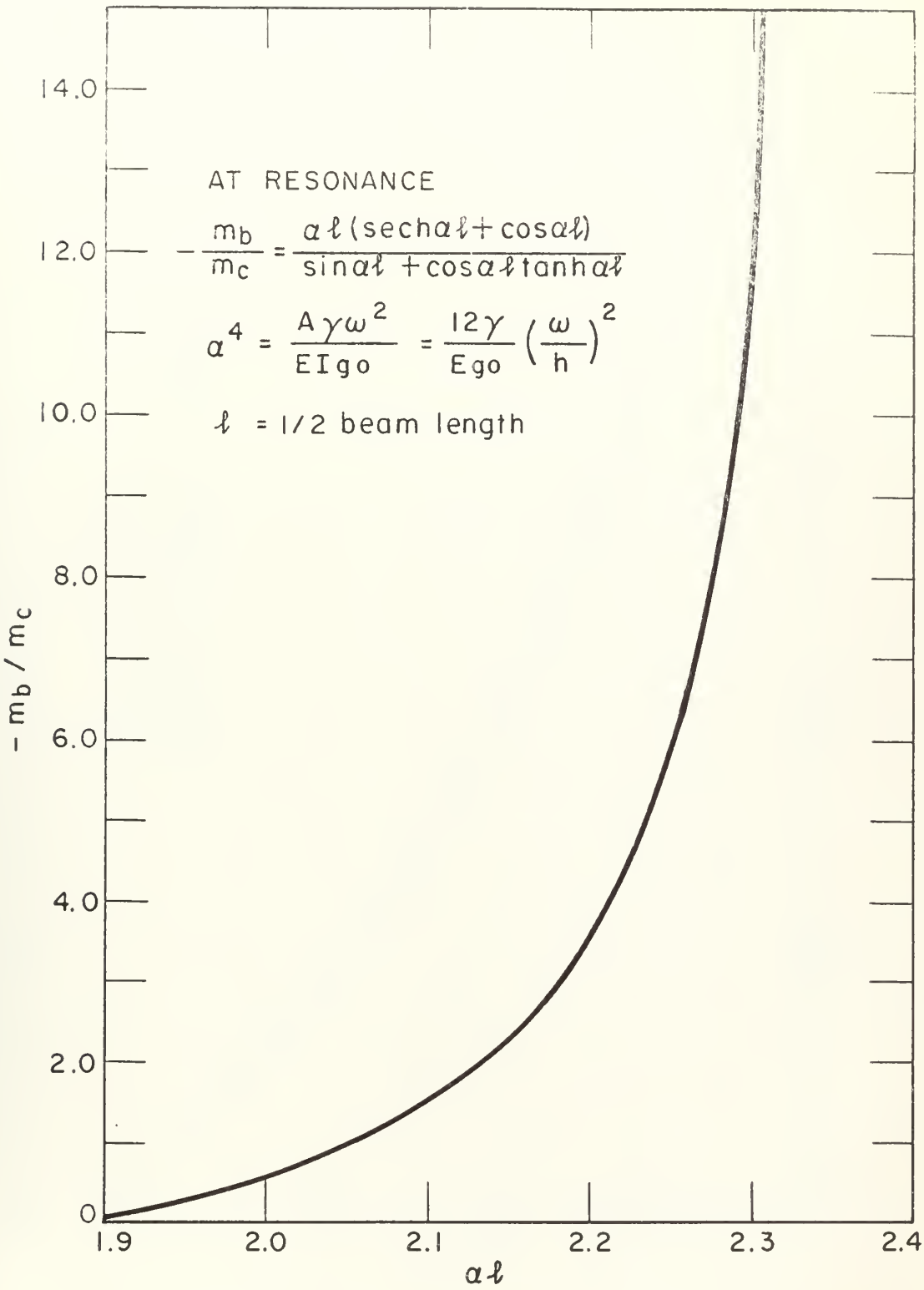

BEAM TO CENTER LOAD MASS RATIO VS $\alpha\ell$ AT RESONANCE

Fig. 6

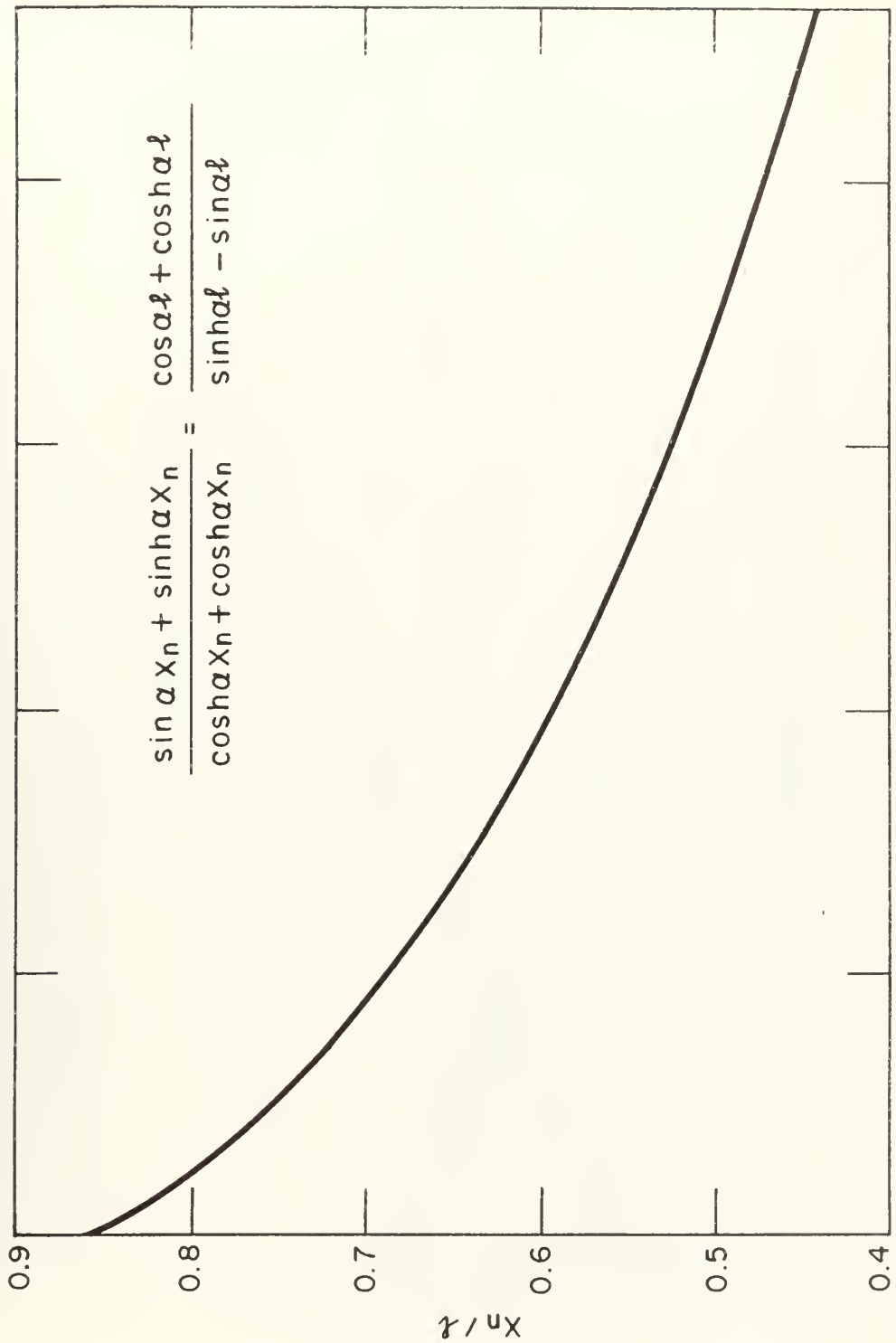

NODAL DISTANCE FROM BEAM END TO HALF BEAM LENGTH RATIO VERSUS $\alpha \ell$

Fig. 7

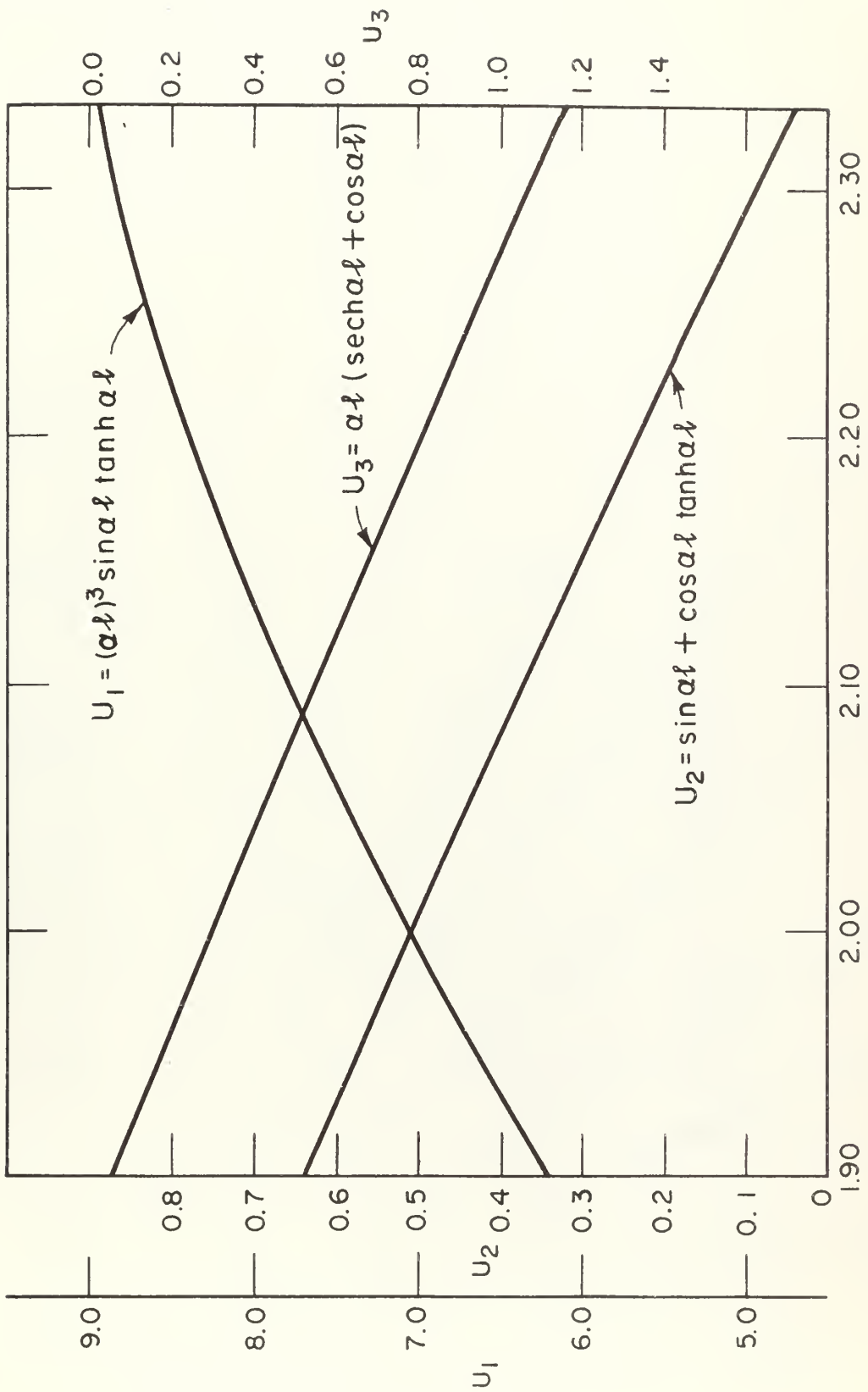
$U_1 = (\alpha l)^3 \sin\alpha l \tanh\alpha l$
$U_3 = \alpha l\,(\operatorname{sech}\alpha l + \cos\alpha l)$
$U_2 = \sin\alpha l + \cos\alpha l \tanh\alpha l$
U_1
U_2
U_3
U_1, U_2 and U_3 versus αl
9.0
8.0
7.0
6.0
5.0
0.8
0.7
0.6
0.5
0.4
0.3
0.2
0.1
0
0.0
0.2
0.4
0.6
0.8
1.0
1.2
1.4
1.90
2.00
2.10
2.20
2.30

Fig. 8

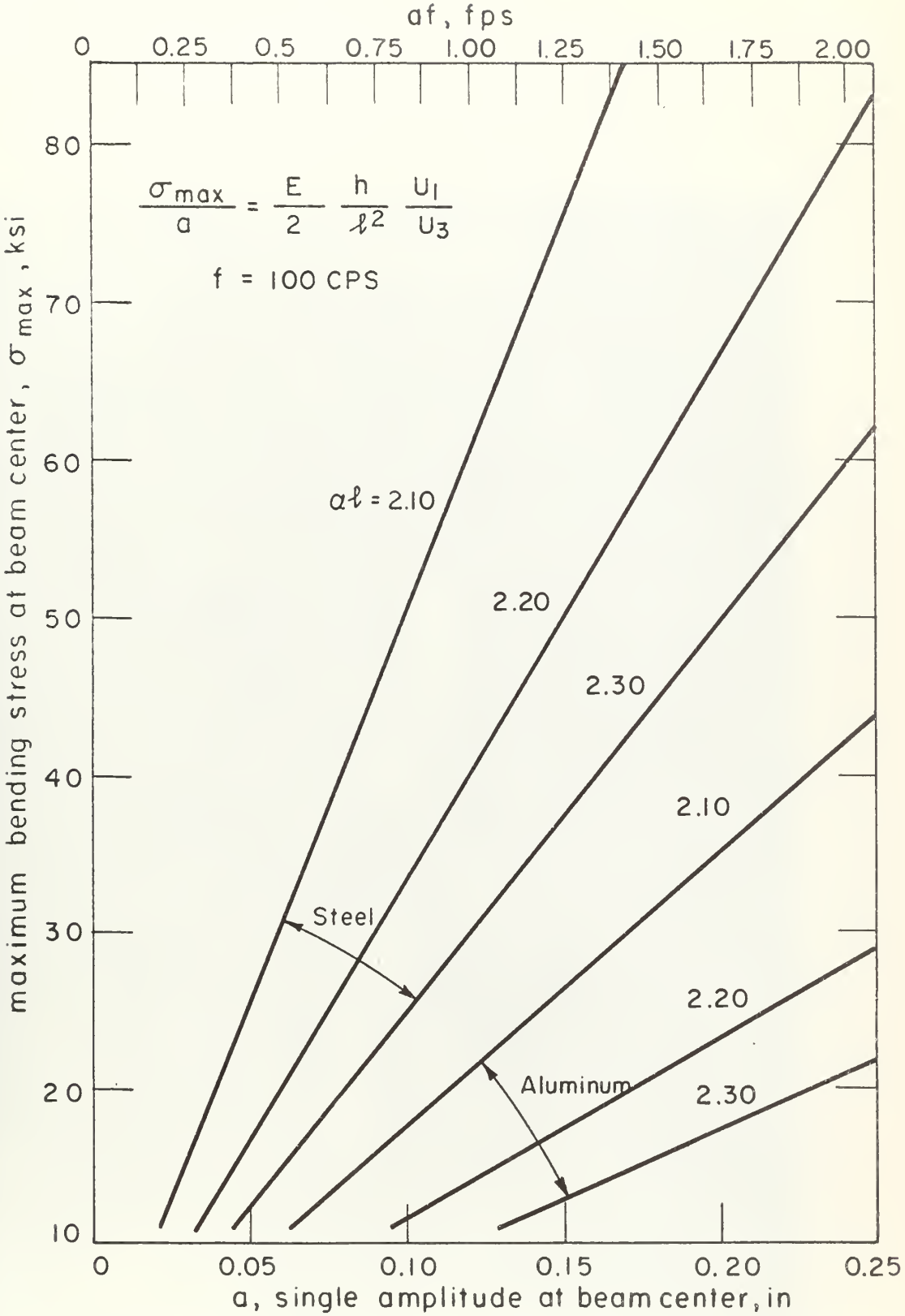

MAXIMUM BENDING STRESS VS AMPLITUDE AND af FOR STEEL AND ALUMINUM BEAMS AT VARIOUS $\alpha\ell$ VALUES WITH A FREQUENCY OF 100 CPS

Fig. 9

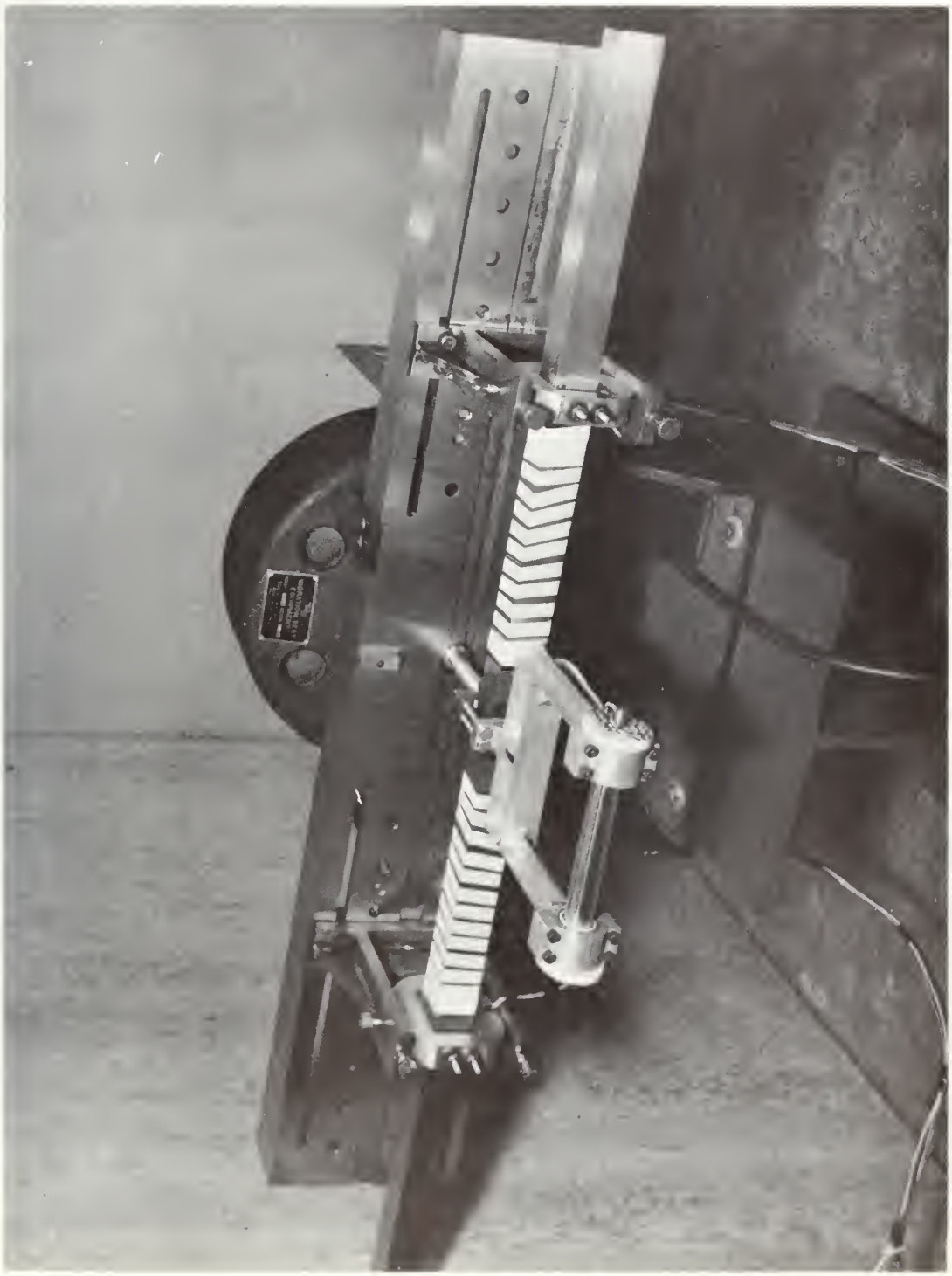

Fig. 10 - Vibration Test Stand, Horizontal Position

Fig. 11 - Close-up View of Test Cylinder

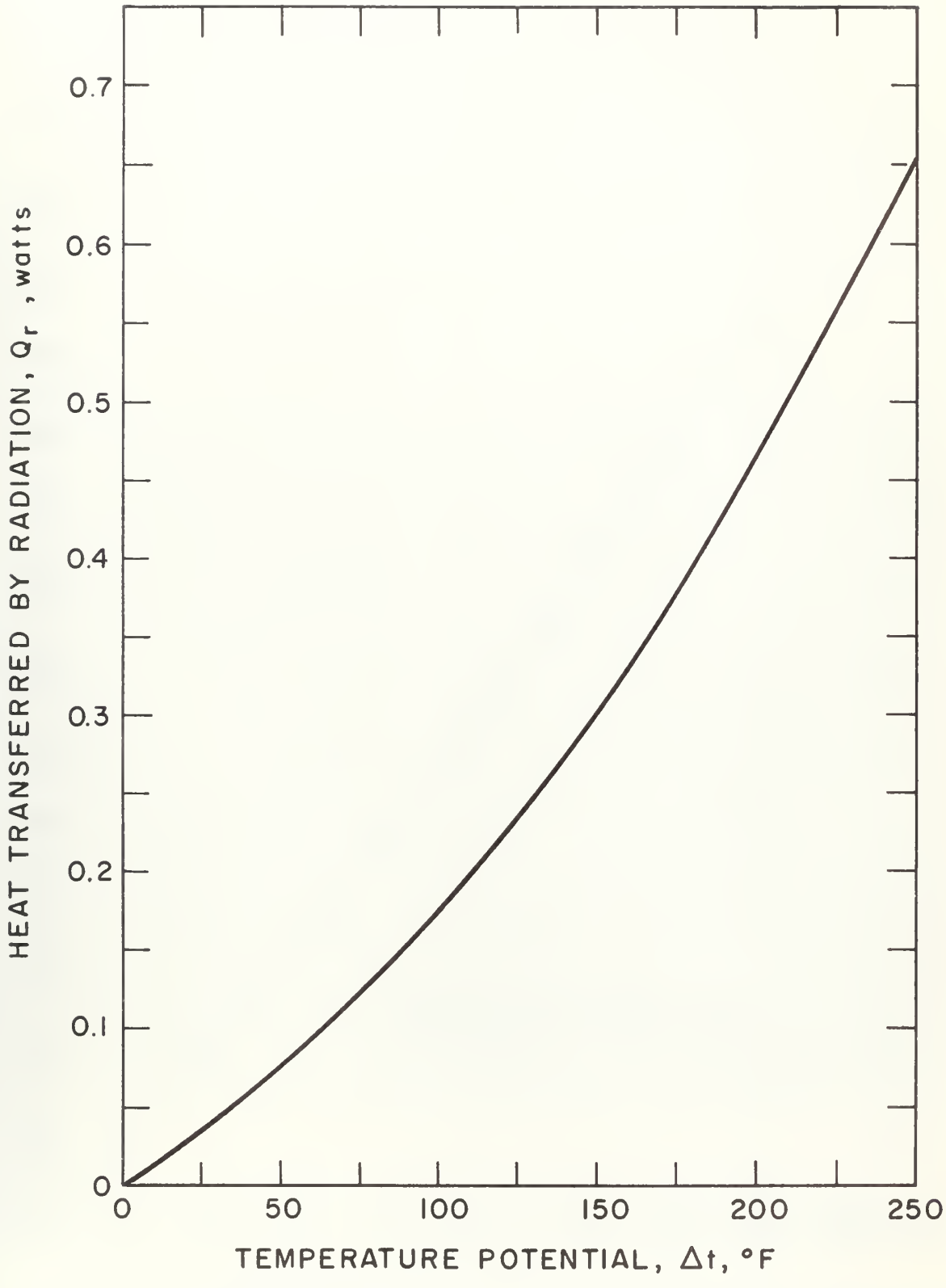

HEAT TRANSFERRED BY RADIATION FROM TEST SECTION

Fig. 12

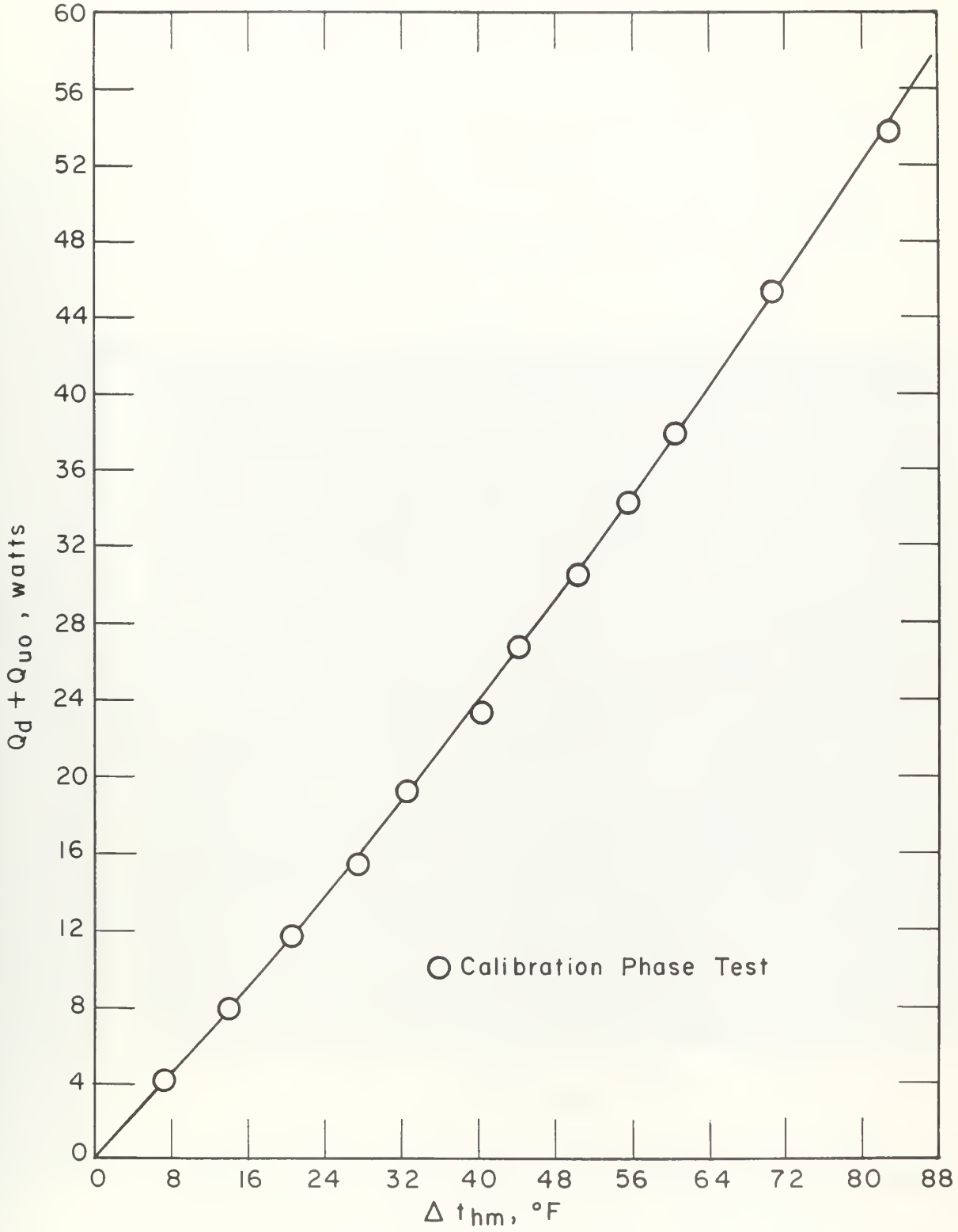

FIG. 13 HEAT TRANSFERRED FROM TEST CYLINDER ENDS, (Q_d+Q_{uo}) VS Δt_{hm}

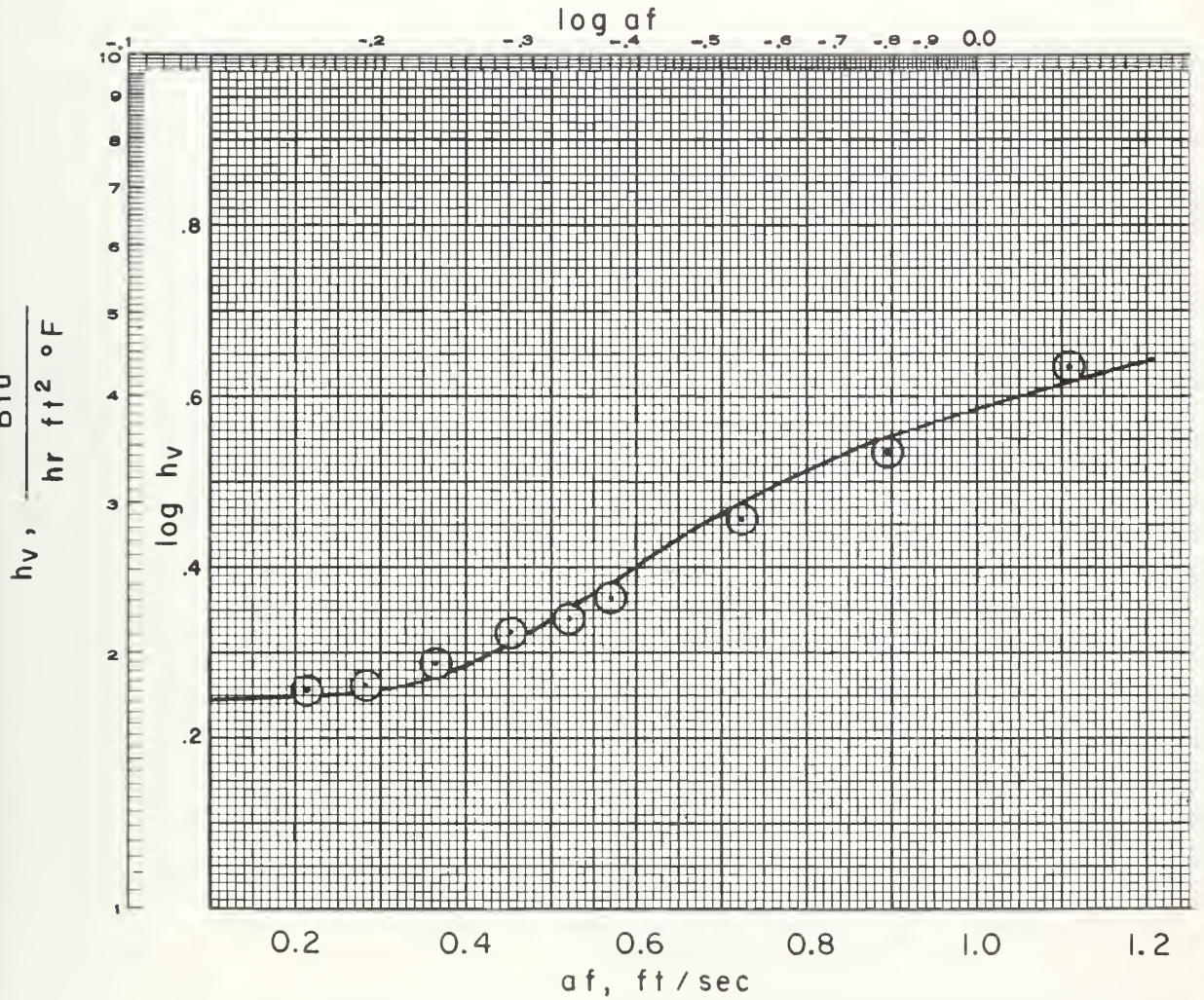

FIG. 14 – COMPARISON OF h_v vs af AT CONSTANT Δt FOR HORIZONTAL CYLINDER IN HORIZONTAL TRANSVERSE MECHANICAL AND ACOUSTICAL VIBRATION

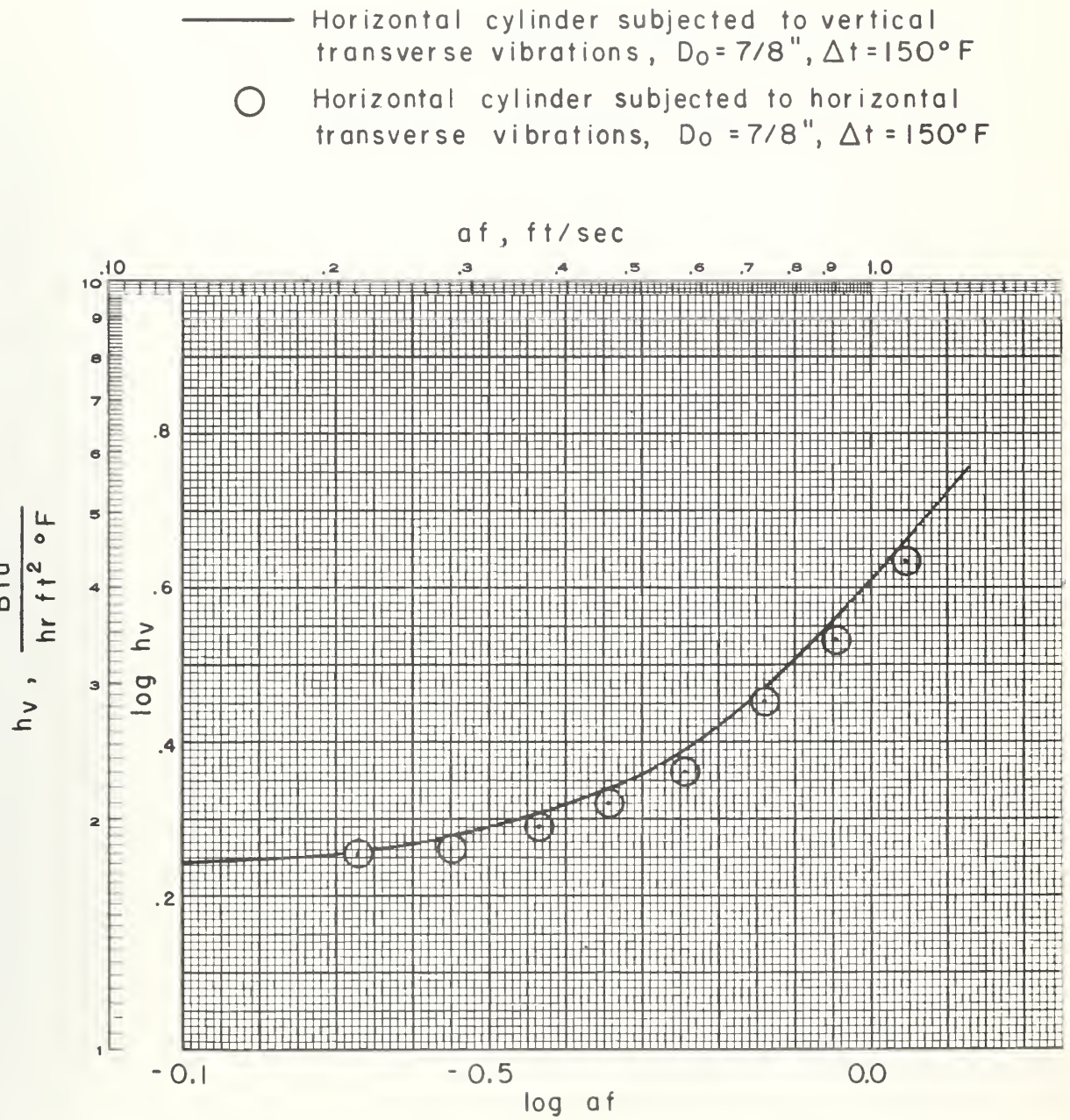

FIG. 15 COMPARISON OF h_v vs af AT CONSTANT Δt FOR HORIZONTAL CYLINDER IN HORIZONTAL AND VERTICAL TRANSVERSE MECHANICAL VIBRATION

TABLES

TABLE 1

EXPERIMENTAL AND COMPUTED VALUES OF CALIBRATION PHASE TESTS

Test No.	Q_m watts	Q_w watts	t_s °F	t_a °F	Δt °F	Q_{co} watts	Q_r watts	$Q_d + Q_{uo}$ watts	Δt_{hm} °F
1	5.00	4.892	101.4	75.8	25.6	0.835	0.038	4.019	7.35
2	10.00	9.784	124.6	75.9	48.7	1.866	0.078	7.480	14.05
3	15.00	14.676	148.4	76.4	72.0	2.994	0.124	11.558	20.66
4	20.00	19.782	163.6	68.8	94.8	4.226	0.171	15.385	27.46
5	25.00	24.727	190.9	76.6	114.3	5.337	0.218	19.172	32.85
6	30.00	29.673	205.3	76.3	129.0	6.213	0.256	23.204	40.44
7	35.00	34.618	228.0	76.2	151.8	7.606	0.319	26.693	44.27
8	40.00	39.564	245.3	76.1	169.2	8.718	0.376	30.470	50.36
9	45.00	44.510	266.7	76.7	190.0	9.809	0.433	34.268	55.67
10	50.00	49.455	282.1	76.4	205.7	11.120	0.504	37.831	60.43
11	60.00	59.346	315.9	76.2	239.7	13.468	0.641	45.237	70.58
12	70.00	69.237	350.6	76.7	273.9	15.912	0.791	52.534	83.01

TABLE 2

EXPERIMENTAL AND COMPUTED VALUES OF VIBRATION PHASE TESTS

Test No.	f cps	a in	af ft/sec	Q_m watts	Q_w watts	Δt °F	Q_r watts	Δt_{hm} °F	$Q_d + Q_{uo}$ watts	Q_{cv} watts	h_v Btu / hr ft² °F
1	104	0.0246	0.213	34.20	33.83	149.97	0.314	43.26	25.65	7.87	1.803
2	104	0.0325	0.281	34.30	33.93	149.45	0.314	43.33	25.68	7.94	1.826
3	104	0.0423	0.367	36.40	36.00	149.40	0.313	45.70	27.25	8.44	1.941
4	104	0.0522	0.452	39.30	38.87	150.86	0.315	48.78	29.35	9.21	2.098
5	104	0.0659	0.571	41.30	40.85	150.24	0.315	50.50	30.55	10.04	2.296
6	104	0.0836	0.725	44.90	44.41	149.66	0.314	52.11	31.63	12.47	2.863
7	104	0.1033	0.895	49.00	48.47	150.99	0.315	54.47	33.51	14.96	3.404
8	104	0.0600	0.520	39.90	39.46	150.10	0.315	48.88	29.60	9.55	2.186
9	104	0.1279	1.109	53.90	53.31	150.24	0.315	55.56	34.10	18.90	4.323

A P P E N D I X

APPENDIX A

VIBRATION ANALYSIS

In the analysis of the free-free beam and coupled center load resonant vibration syste, it was assumed that the exciter moving element, the test cylinder and its supporting yoke and the hardware used in coupling the exciter moving element to the beam acted as a concentrated mass of magnitude m_c at the beam center. The beam had a length 2ℓ and a total mass m_b. The coordinates used in the analysis are as shown below.

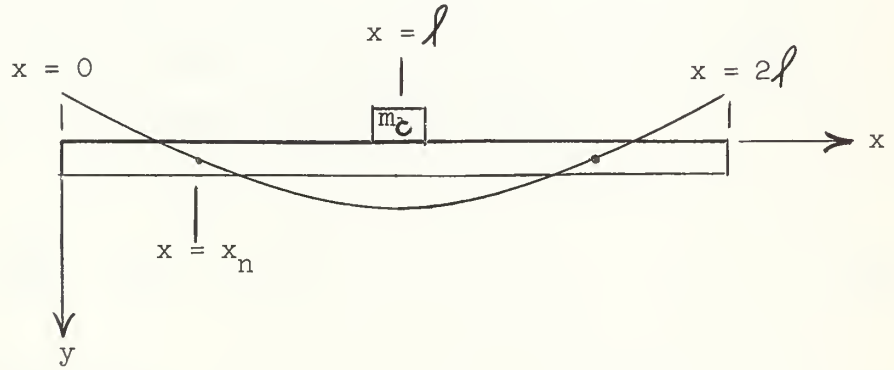

The general equation for the transverse vibration of a prisimatical beam, as presented by Timoshenko[13] is:

$$EI \frac{d^4y}{dx^4} = - \frac{\gamma A}{g_o} \frac{d^2y}{dt^2} \qquad (15)$$

which may be written:

$$\frac{d^2y}{dt^2} + \frac{EIg_o}{A\gamma} \frac{d^4y}{d^4x} = 0 \qquad (16)$$

where

E = modulus of elasticity, lb/in^2

I = beam cross-sectional moment of inertia, in^4

g_o = gravitational constant, 386 in/sec^2

γ = beam weight density, lb/in^3

Considering only the first mode of vibration as was justified in Chapter III, Section 1-b, the solution to Equation (16) has the form $y = X \sin \omega t$, where $\sin \omega t$ gives the periodic variation of the beam deflection along its length according to the function X = f(x). Substituting this solution into Equation (16) yields:

$$\frac{d^4X}{dx^4} - \alpha^4 X = 0 \qquad (17)$$

where α is defined by:

$$\alpha^4 = \frac{A\gamma\omega^2}{EIg_o} \qquad (18)$$

Particular solutions of Equation (18) involve the functions $\sin\alpha x$, $\cos\alpha x$, $\sinh\alpha x$ and $\cosh\alpha x$. Therefore, the solution to Equation (16) can be conveniently expressed as:

$$y = X \sin\omega t = \left[C_1 (\cos\alpha x + \cosh\alpha x) + C_2 (\cos\alpha x - \cosh\alpha x) + C_3 (\sin\alpha x + \sinh\alpha x) + C_4 (\sin\alpha x - \sinh\alpha x)\right] \sin\omega t \qquad (19)$$

Application of the end boundary conditions, i.e., the bending moment $EI \frac{d^2y}{dx^2}$ and shear force $EI \frac{d^3y}{dx^3}$ vanish at $x = 0$ and $x = 2\ell$, reveals that $C_2 = C_4 = 0$. Similarly, the mid-span boundary condition of zero slope, $\frac{dy}{dx} = 0$ at $x = \ell$, gives:

$$C_1 = \frac{\cos\alpha\ell + \cosh\alpha\ell}{\sin\alpha\ell - \sinh\alpha\ell} C_3 \tag{20}$$

An additional condition at beam center is obtained from the force-inertia balance at $x = \ell$:

(a) Exciter force (up): $F = F_o \sin\omega t$

(b) Shear force (up): $2EI \frac{d^3y}{dx^3}$

(c) Inertia load of m_c (down): $- m_c \frac{d^2y}{dt^2}$

Thus, at $x = \ell$:

$$F_o \sin\omega t + 2EI \frac{d^3y}{dx^3} = m_c \frac{d^2y}{dt^2} \tag{21}$$

Substitution of Equations (19) and (20) into Equation (21) results in the following:

$$F + 2EI\alpha^3 C_3 \left[- \cos\alpha\ell + \cosh\alpha\ell + (\sin\alpha\ell + \sinh\alpha\ell) \frac{\cos\alpha\ell + \cosh\alpha\ell}{\sin\alpha\ell - \sinh\alpha\ell} \right]$$

$$= - m_c \omega^2 C_3 \left[\sin\alpha\ell + \sinh\alpha\ell + \frac{(\cos\alpha\ell + \cosh\alpha\ell)^2}{\sin\alpha\ell - \sinh\alpha\ell} \right] \tag{22}$$

Also, from the definition of α the beam mass, m_b, may be conveniently introduced into Equation (22) as follows:

$$2EI\alpha^3 = \frac{2EI}{\alpha}\left(\frac{A\gamma\omega^2}{EIg_o}\right) = \frac{m_b\omega^2}{2\alpha\ell} \tag{23}$$

For convenience, the first and second terms in brackets of Equation (22) are called Q and R. Substituting Equation (23 into (22) gives:

$$C_3 = \frac{-F}{m_c\omega^2 Q\left(\frac{1}{\alpha\ell}\frac{m_b}{m_c} + \frac{R}{Q}\right)} \tag{24}$$

Examination of Equations (19) and (22) shows that beam displacement, y, is a function of C_3 and $\alpha\ell$. At the theoretical resonance condition, y becomes infinite. However, for a finite frequency and a beam of finite mass and dimensions, $\alpha\ell$ cannot approach infinity. Hence, with regard to theory, C_3 must become infinite at resonance. Therefore, the denominator of the right-hand side of Equation (24) must vanish at resonance, and:

$$-\frac{m_b}{m_c} = \alpha\ell\,\frac{R}{Q} \tag{25}$$

Substitution of the bracket terms Q and R and simplifying produces the following frequency equation in terms of beam to center mass ratio at resonance:

$$-\frac{m_b}{m_c} = \frac{\alpha\ell\,(\operatorname{sech}\alpha\ell + \cos\alpha\ell)}{(\sin\alpha\ell + \cos\alpha\ell\,\tanh\alpha\ell)} \tag{26}$$

Equation (26) is plotted for various mass ratios versus values of $\alpha\ell$ in Fig. 6. It is worthwhile to note that the first mode solution of the simple free-free beam with no added center-span mass should correspond to the value of $\alpha\ell$ as m_b/m_c approaches infinity. Reference 14 gives the frequency solution for this case as:

$$\omega = 22.4 \sqrt{\frac{EIg_o}{A\gamma(2\ell)^4}} \tag{27}$$

Substitution for α into Equation (27) and solving for $\alpha\ell$ gives a value of $\alpha\ell = 2.37$ at resonance. Fig. 6 clearly indicates that approaches 2.37 as m_b/m_c approaches infinity.

In order to have minimum force transmission from the beam to the beam supports, these supports must be located at the vibration nodal points. Solving for beam deflection, y, by substituting Equation (20) into (19):

$$y = \left[\frac{\cos\alpha\ell + \cosh\alpha\ell}{\sin\alpha\ell - \sinh\alpha\ell}(\cos\alpha x + \cosh\alpha x) + (\sin\alpha x + \sinh\alpha x)\right] \cdot C_3 \sin\omega t = 0 \tag{28}$$

At the nodes, say at $x = x_n$, $y = 0$. Equating Equation (28) to zero gives:

$$\frac{\sin\alpha\ell\frac{x_n}{\ell} + \sinh\alpha\ell\frac{x_n}{\ell}}{\cos\alpha\ell\frac{x_n}{\ell} + \cosh\alpha\ell\frac{x_n}{\ell}} = \frac{\cos\alpha\ell + \cosh\alpha\ell}{\sinh\alpha\ell - \sin\alpha\ell} \tag{29}$$

The ratio of nodal distance from beam end to beam half length, x_n/ℓ, is plotted versus $\alpha\ell$ in Fig. 7.

The maximum bending moment in the beam will occur at $x = \ell$ when the center amplitude, a, is at its maximum value. This will take place at times when $\sin\omega t$ is unity. From elementary beam theory, the bending moment is given by $M = EI \frac{d^2y}{dx^2}$; thus, differentiating Equation (28) twice:

$$M_{max} = EI \left.\frac{d^2y}{dx^2}\right|_{x=\ell} = 2EI\alpha^2 C_3 \left(\frac{\sin\alpha\ell \sinh\alpha\ell}{\sin\alpha\ell - \sinh\alpha\ell}\right) \quad (30)$$

The maximum stress, σ_{max}, is given by M_{max}/I times h/2 where h is the beam height in the direction of deflection. Combining this with Equations (24 and (28) gives:

$$\sigma_{max} = E \frac{F}{2m_c} \frac{h}{\ell^2} \frac{1}{\omega^2} \frac{U_1}{\frac{m_b}{m_c} U_2 + U_3} \quad (31)$$

where

$$U_1 = (\alpha\ell)^3 \sin\alpha\ell \tanh\alpha\ell \quad (32)$$

$$U_2 = \sin\alpha\ell + \cos\alpha\ell \tanh\alpha\ell \quad (33)$$

$$U_3 = \alpha\ell (\operatorname{sech}\alpha\ell + \cos\alpha\ell) \quad (34)$$

U_1, U_2 and U_3 are plotted versus $\alpha\ell$ in Fig. 8.

The maximum amplitude at $x = \ell$ is given by Equation (28) for times when $\sin\omega t$ is unity. Upon substitution for C_3:

$$a = \frac{F}{m_c} \frac{1}{\omega^2} \frac{U_3}{\frac{m_b}{m_c} U_2 + U_3} \tag{35}$$

Equations (31) and (35) are not useful at resonance because the denominator term $\frac{m_b}{m_c} U_2 + U_3$ vanishes at the resonant condition. This is a result of the earlier assumption that maximum amplitude goes to infinity at resonance, i.e., C_3 approaches infinity at resonance. However, the ratio of bending moment to amplitude may be obtained by dividing Equation (31) by (35), and:

$$\frac{\sigma_{max}}{a} = \frac{E}{2} \frac{h}{\ell^2} \frac{U_1}{U_3} \tag{36}$$

The maximum bending stress versus amplitude and vibration intensity, af, for steel and aluminum beams at various $\alpha\ell$ values and at f = 100 cps is plotted in Fig. 9.

The interpretation of this analysis and final beam selection is presented in Chapter III, Section 1-b. The curves developed by means of this analysis (Figs. 6, 7, 8 and 9) were used for final beam design according to the calculation method indicated in Appendix B. It is considered that this analysis served as a remarkably useful tool in this project. The resonant frequency obtained of the actual beam was within 1 1/2 per cent of the design value.

APPENDIX B

RESONANT BEAM DESIGN CALCULATIONS

The resonant free-free beam design calculations based on the analysis presented in Appendix A are given below. Beam width, b, was initially set at 1.50" so that existing hardware for test cylinder support could be employed. The material selected, "HY-100" steel, had a weight density of 0.283 lb/in^3. As explained in Chapter II, Section 1-b, a value of $\alpha\ell = 2.25$ was selected for the final design on the basis of stress and beam size considerations. The weight of the center span load, consisting of the test cylinder and test cylinder yoke, exciter extension and coupling hardware, and the exciter moving element, was estimated to be $W_c = 5.5$ lbs. Thus, for $\alpha\ell = 2.25$

$$\frac{m_b}{m_c} = \frac{W_b}{W_c} = 5.76 \text{ from Fig. 6}$$

and

$$W_b = 5.76 \times 5.5 = 31.68 \text{ lbs}$$

also

$$W_b = b \times h \times 2\ell \times \gamma = 31.68 \text{ lbs}$$

Another equation for ℓ in terms of h may be obtained from Equation (18), Appendix A:

$$\alpha^4 = \frac{A\gamma\omega^2}{EIg_o} = \frac{12\gamma}{Eg_o}\left(\frac{2\pi f}{h}\right)^2$$

Then

$$\alpha\ell = \left[\frac{12\gamma}{Eg_o}\left(\frac{2\pi f}{h}\right)^2\right]^{1/4}\ell = 2.25$$

Squaring both sides of this equation gives:

$$\left(\frac{12\gamma}{Eg_o}\right)^{1/2} (2\pi f) \frac{\ell^2}{h} = (2.25)^2$$

where

$f = 100$ cps

$E = 30 \times 10^6$ lb/in^2

$g_o = 386$ in/sec^2

thus

$$\left(\frac{12 \times 0.283}{30 \times 10^6}\right)^{1/2} (2\pi \times 100) \frac{\ell^2}{h} = (2.25)^2$$

$$\frac{\ell^2}{h} = 475, \text{ or } h = \frac{\ell^2}{475}$$

Substitution of this relation for h into the above expression for W_b gives:

$$W_b = b \times h \times 2\ell \times \gamma = 31.68 = b \times \frac{\ell^2}{475} \times 2\ell \times \gamma$$

Thus ℓ may be calculated:

$$1.5 \times \frac{\ell^2}{475} \times 2\ell \times 0.283 = 31.68$$

$$\ell^3 = \frac{31.68 \times 475}{1.5 \times 2 \times 0.283}$$

$$\ell = 26.07"$$

Beam length $= 2\ell = 52.14"$

Since $h = \ell^2/475$:

$$h = \frac{(26.07)^2}{475} = 1.43"$$

The steel beam dimensions for a resonant frequency of 100 cps with a center load of 5.5 lbs are:

$$1.50" \times 1.43" \times 52.14" \quad .$$

The steel beam as machined had the following dimensions:

$$1.475" \times 1.408" \times 52.20" \quad .$$

The resonant frequency of this beam was determined as follows:

$$W_b = 0.283 \times 1.474 \times 1.408 \times 52.20 = 30.717 \text{ lbs}$$

$$W_c = 5.50 \text{ lbs}$$

$$\frac{m_b}{m_c} = \frac{W_b}{W_c} = \frac{30.717}{5.50} = 5.585$$

From Fig. 6, for $m_b/m_c = 5.585$, $\alpha\ell = 2.247$; hence:

$$\alpha = \frac{\alpha\ell}{\ell} = \frac{2.247}{26.10} = 0.0861$$

$$\alpha = \left[\frac{12\gamma}{Eg_o} \left(\frac{2\pi f}{h}\right)^2 \right]^{1/4} = 0.0861$$

$$\frac{12 \times 0.283}{30 \times 10^6 \times 386} \left(\frac{2\pi f}{1.408}\right)^2 = (0.0861)^4$$

and

$$f = 97.0 \text{ cps}$$

It was desired to have a minimum resonant frequency of 100 cps, however. The calculated resonant frequency was raised to 105.3 cps by shortening the beam to a length of 50.00". Thus, the above calculation procedure is used again, as:

$$W_b = 0.283 \times 1.474 \times 1.408 \times 50.00 = 29.367 \text{ lbs}$$

$$\frac{m_b}{m_c} = \frac{29.367}{5.5} = 5.340, \quad \alpha\ell = 2.243 \text{ from Fig 6}$$

$$\alpha = \frac{2.243}{25.00} = .0897 = \left(\frac{12\gamma}{Eg_o}\right)^{1/4} \left(\frac{2\pi f}{h}\right)^2$$

from which

$$f = 105.3 \text{ cps.}$$

The actual experimental resonant frequency of the system was 104 cps.

The nodal distance from beam end, x_n, was determined from Fig. 7 with the value of $\alpha\ell = 2.243$:

$$\text{for } \alpha\ell = 2.243, \quad \frac{x_n}{\ell} = 0.503$$

$$\text{since } \ell = 25.00"$$

$$x_n = 25 \times 0.503 = 12.575"$$

Each gimbal assembly was then placed this distance from each beam end.

APPENDIX C

CALIBRATION PHASE HEAT TRANSFER SAMPLE CALCULATIONS

The calculations presented below were those performed for calibration phase Test No. 9 (Table 1) which had the following relevant original data:

Q_m = 45.00 watts

t_s = 266.7°F

t_a = 76.7°F

a. t, temperature potential

Formula: $\Delta t = t_s - t_a$

t_s = 266.7°F

t_a = 76.7°F

Δt = 266.7 - 76.7 = 190.0°F

b. Q_w, power delivered to test section

Formula: $Q_w = 0.9891\ Q_m$

Q_m = 45.00 watts

Q_w = 0.9891 x 45.00 = 44.510 watts

c. Q_r, heat transferred by radiation

Method: Q_r = value read from Fig. 12, corresponding to Δt

Δt = 190.0°F

Q_r = 0.433 watts

d. Q_{co}, heat transferred by free convection in absence of vibration

Formula: $Q_{co} = 0.01428 \Delta t^{5/4}$, watts

$t = 190.0^{o}F$, $t^{5/4} = 686.804$

$Q_{co} = 0.01428 \times 686.804 = 9.809$ watts

e. $Q_d + Q_{uo}$, axial heat loss from test cylinder

Formula: $Q_d + Q_{uo} = Q_w - (Q_r + Q_{co})$

$Q_w = 44.510$ watts

$Q_r = 0.433$ watts

$Q_{co} = 9.809$ watts

$Q_d + Q_{uo} = 44.510 - (0.433 + 9.809)$

$Q_d + Q_{uo} = 34.268$ watts

APPENDIX D

VIBRATION PHASE HEAT TRANSFER SAMPLE CALCULATIONS

The calculations presented below were those performed for vibration phase Test No. 6 (Table 2) which had the following relevant original data:

$f = 104$ cps

$Q_m = 44.90$ watts

$a = 0.0836"$

$\Delta t_{hm} = 52.11^{\circ}F$

$t_s = 228.03^{\circ}F$

$t_a = 78.37^{\circ}F$

a. t, temperature potential

Formula: $\Delta t = t_s - t_a$

$t_s = 228.03^{\circ}F$

$t_a = 78.37^{\circ}F$

$\Delta t = 228.03 - 78.37 = 149.66^{\circ}F$

b. Q_w, power delivered to test section

Formula: $Q_w = 0.9891\ Q_m$

$Q_m = 44.90$ watts

$Q_w = 0.9891 \times 44.90 = 44.41$ watts

c. Q_r, heat transferred by radiation

Method: Q_r = value read from Fig. 12, corresponding to Δt

$\Delta t = 149.66^{\circ}F$

$Q_r = 0.314$ watts

d. $Q_d + Q_{uo}$, axial heat loss from test cylinder

Method: $Q_d + Q_{uo}$ = value read from Fig. 13, corresponding to

$$\Delta t_{hm}$$

$\Delta t_{hm} = 52.11^{o}F$

$Q_d + Q_{uo} = 31.63$ watts

e. Q_{cv} , heat transferred by convection in presence of vibration

Formula: $Q_{cv} = Q_w - Q_r - (Q_d + Q_{uo})$

$Q_w = 44.41$ watts

$Q_r = 0.314$ watts

$Q_d + Q_{uo} = 31.63$ watts

$Q_{cv} = 44.41 - 0.31 - 31.63 = 12.47$ watts

f. h_v, heat-transfer coefficient in presence of vibration

Formula: $h_v = 3.412 \dfrac{Q_{cv}}{A \Delta t}$

$Q_{cv} = 12.47$ watts

$A = 0.0993\ ft^2$

$\Delta t = 149.66^{o}F$

$$h_v = 3.412 \times \frac{12.47}{0.0993 \times 149.66} = 2.863 \ \frac{Btu}{hr\ ft^2\ {}^{o}F}$$

g. af, the intensity of vibration

Formula: $af = \dfrac{a \times f}{12}$

$a = 0.0836"$

$f = 104$ cps

$$af = \frac{0.0836 \times 104}{12} = 0.725 \text{ ft/sec}$$

APPENDIX E

BIBLIOGRAPHY

1. Raben, I. and Dietert, R., "An Investigation of the Use of Acoustic Vibrations to Improve Heat Transfer Rates and Reduce Scaling in Distillation Units used for Saline Water Conversion," Southwest Research Inst. Proj. 2-919-1 Progress Reports 1 through 3. Jan. to June 1960.

2. Westervelt, P. J., "Hydrodynamic Flow and Oseen's Approximations," Journal, Acoustical Society of America, Vol. 25, 1953, p. 951.

3. Martinelli, R. C., and Boelter, L. M. K., "The Effect of Vibrations Upon the Free Convection from a Horizontal Tube," Proceedings, Fifth International Congress of Applied Mechanics, 1938, p. 578.

4. Lemlich, R., "Effect of Vibration on Natural Convection Heat Transfer," Symposium on Pulsatory and Vibrational Phenomena, Industrial and Eng. Chem., Vol. 47, No. 6, 1955.

5. Tsui, Y. T., The Effect of Vibrations on Heat Transfer Coefficients. Ph.D. Thesis, Ohio State University, 1953.

6. Shine, A. J., The Effect of Transverse Vibrations on the Heat Transfer Rate from a Heated Vertical Plate. M.S. Thesis, Air Inst. of Techn. Wright-Patterson Air Force Base, Ohio, 1957.

7. Freedman, S. I., The Effect of Small Vibrations on Free Convective Heat Transfer from Vertical Cylinders. S.M. Thesis, M.I.T. Dept.of M. E., 1957.

8. Teleki, C., Fand, R. M., Kaye, J., "The Influence of Vertical Vibrations on the Rate of Heat Transfer from a Horizontal Cylinder in Air," USAF, WADC TN 59-357.

9. Fand, R. M. and Kaye, J., "The Influence of Vertical Vibrations on Heat Transfer by Free Convection from a Horizontal Cylinder, " Paper A-17, International Heat Transfer Conference, Boulder, Colo., August, 1961.

10. Fand, R. M. and Kaye, J., "The Effect of High Intensity Stationary and Progressive Sound Fields on Free Convection from a Horizontal Cylinder," USAF, WADC TN 59-18, 1959.

11. Fand, R. M. and Kaye, J., "Acoustic Streaming Near a Heated Cylinder," Journal, Acoustical Society of America, Vol. 32, 1960, p. 579.

12. McAdams, W. H., Heat Transmission, McGraw-Hill, New York, 3, 1954.

13. Timoshenko, S., Vibration Problems in Engineering, D. Van Nostrand Co., Inc., New York 3, 1955.

14. Den Hartog, J. P., Mechanical Vibrations, McGraw-Hill, New York, 4, 1956.

15. Lewis, R. C., "Test Techniques Using Electro-Dynamic Shakers," Products Engineering, January, 1951.